Univerzita Karlova
Přírodovědecká fakulta

Studijní program: Chemie

Paulína Šimková

Chování polyelektrolytů ve vodných roztocích zkoumané rozptylovými technikami
Polyelectrolyte behavior in solution as seen by scattering techniques

BAKALÁŘSKÁ PRÁCE

Vedoucí bakalářské práce: Ing. Mariusz Uchman, Ph.D.
Konzultanti bakalářské práce: prof. RNDr. Miroslav Štěpánek, Ph.D.
Ing. Katarzyna Byś

Praha, 2024

Prohlašuji, že jsem tuto bakalářskou práci vypracoval(a) samostatně a výhradně s použitím citovaných pramenů, literatury a dalších odborných zdrojů. Tato práce ani její podstatná část nebyla předložena k získání jiného nebo stejného akademického titulu. Beru na vědomí, že se na moji práci vztahují práva a povinnosti vyplývající ze zákona č. 121/2000 Sb., autorského zákona v platném znění, zejména skutečnost, že Univerzita Karlova má právo na uzavření licenční smlouvy o užití této práce jako školního díla podle §60 odst. 1 autorského zákona.

V ..... dne ....

Podpis autora

This thesis would not be possible without my consultant Ing. Katarzyna Byś. I would like to extend my deepest gratitude for her guidance, patience, insightful discussions, continuous support, encouragement and help throughout the whole process of experimental part and writing. My sincere thanks go to my consultant prof. RNDr. Miroslav Štěpánek, Ph.D. for fruitful discussions, suggestions and major help with small-angle X-ray scattering. Last, but not least I would like to thank my supervisor Ing. Mariusz Uchman, Ph.D. for his advice and assistance. I am thankful to all group members. I want to thank Ing. Jan Stránský, Ph.D. for help and technical assistance with small angle X-ray scattering. My heartfelt thanks also go to my boyfriend, brother, parents and friends, who have been with me through thick and thin. Without their encouragement, this would not be possible.

Název práce: Chování polyelektrolytů ve vodných roztocích zkoumané rozptylovými technikami

Autor: Paulína Šimková

Katedra fyzikální a makromolekulární chemie: Přírodovědecká fakulta

Vedoucí bakalářské práce: Ing. Mariusz Uchman, Ph.D., Katedra fyzikální a makromolekulární chemie

Abstrakt: Předložená práce zkoumá chování tří polyelektrolytů odvozených od společného prekurzoru, polyisoprenu: poly((sulfamát-karboxylát)isopren), poly((amino-karboxylát)isopren) a poly((trimethylamonium-karboxylát)isopren) s různými molárními hmotnostmi - 7,5; 38 a 75,5 kDa. Tyto polyelektrolyty jsou zkoumány ve zředěných vodných roztocích při konstantní iontové síle v celém rozsahu pH, aby byly prozkoumány různé ionizační stavy. Charakterizační techniky zahrnují dynamický a statický rozptyl světla (DLS a SLS), maloúhlový rozptyl rentgenového záření (SAXS) a měření zeta potenciálu. Molekulová hmotnost ovlivňuje velikosti vytvořených asociátů. Krátké polyelektrolyty tvoří větší částice kvůli nedostatku možností stabilizace. Dlouhé polyelektrolyty tvoří menší částice z důvodu možné konformační stabilizace. Očekávané účinky pH na velikost částic nebyly potvrzeny.

Klíčová slova: Polyelektrolyty, rozptyl světla, zeta-potenciál, samoorganizace

Title: Polyelectrolyte behavior in solution as seen by scattering techniques

Author: Paulína Šimková

Department of Physical and Macromolecular Chemistry: Faculty of Science

Supervisor: Ing. Mariusz Uchman, Ph.D., Department of Physical and Macromolecular Chemistry

Abstract: This thesis investigates the behavior of three polyelectrolytes derived from a common precursor, polyisoprene: poly((sulfamate-carboxylate)-isoprene), poly((amino-carboxylate)isoprene), and poly((trimethylammonium-carboxylate)isoprene) with varying molar masses - 7.5, 38 and 75.5 kDa. These polyelectrolytes are examined in dilute aqueous solutions at constant ionic strength across a range of pH conditions to explore different ionization states. Characterization techniques include dynamic and static light scattering (DLS and SLS), small-angle X-ray scattering (SAXS), and zeta potential measurements. The molecular weight affects sizes of formed associates. The short polyelectrolytes form bigger particles due to the lack of stabilization opportunities. The long polyelectrolytes form smaller particles, because of possible conformational stabilization. The expected effects of pH on the size of particles were not confirmed.

Keywords: Polyelectrolytes, light scattering, zeta-potential, self-assembly

List of Abbreviations

AC	Absorption capacity
ATRP	Atom transfer radical polymerization
CONTIN	Constrained regularization method for inverting data
DLS	Dynamic light scattering
LS	Light scattering
NR	Natural rubber
NMP	Nitroxide mediated polymerization
PACIS	Poly((amino-carboxylate)isoprene)
PA	Polyampholyte
PE	Polyelectrolyte
PIS	cis-1,4-polyisoprene
PISC	Poly((sulfamate-carboxylate)isoprene)
PZ	Polyzwitterion
RAFT	Reversible addition-fragmentation chain transfer polymerization
SANS	Small angle neutron scattering
SAXS	Small angle X-ray scattering
SLS	Static light scattering
qPACIS	Poly((trimethylammonium-carboxylate)isoprene)
ZP	Zeta potential

Contents

List of Abbreviations **iv**

Introduction **2**

1 Literature overview **3**
1.1 Polyelectrolytes 3
1.1.1 Block polyelectrolytes 8
1.1.2 Brief look at synthesis of polyelectrolytes 9
1.2 Characterization methods 9
1.2.1 Light scattering 10
1.2.2 Small angle X-ray scattering 14
1.2.3 Zeta potential 17

2 Aim of the thesis **19**

3 Materials and used methods **20**
3.1 Studied polyelectrolytes 20
3.2 Sample preparation 21
3.3 Instrument specifications 21
3.3.1 Light scattering 21
3.3.2 SAXS 22
3.3.3 Zeta potential 22

4 Results and discussion **23**
4.1 Ionic properties of studied polyelectrolytes 23
4.2 Associates size determination by dynamic and static light scattering measurements 24
4.3 Associates size determination by static light and small angle X-ray scattering 36
4.4 Associates zeta potential determination 38

Conclusion **41**

References **43**

List of Figures **48**

List of Tables **49**

Introduction

Polyelectrolytes are substances that many scientists are working on and trying to clarify their complex behavior. They are challenging for experimental and theoretical researchers. Moreover, the synthesis of functional polyelectrolytes is a very demanding task. Among the interesting properties belong pH-responsive behavior (which is the topic of this thesis), thermoresponsive behavior and much more.

In general, polyelectrolytes have promising applications in many fields and can be used in optics as contact lenses or even in electrooptics.[1] Other up-and-coming use is for controlled-release drug delivery, tissue engineering, implants or even some systems can respond to specific substances, which can be used for biosensors. Another utilization for day-to-day life is in hygiene products as baby diapers or feminine incontinence products. Materials used for this application are called superabsorbent polymers, which are known because of their high swelling capacity.[2][3][4][5][6] Moreover, polyelectrolytes occur commonly in nature, as for example RNA, DNA, polypeptides, proteins and cellulose derivatives.[7] Although they are a common part of our everyday life, there is much about them to discover. Better understanding of PEs can lead to progress also in other fields than just chemistry, but also medicine, biomedicine or biophysics.

The particle size and characterization of particles (specifically nanoparticles) shape is a crucial factor for biological or biomedical applications. The mentioned particle size influences permeation through biological membranes, which is significant for drug delivery systems. The pharmaceutical applications increasingly include nanoparticles to the formulation process due to the advantages, which those carriers provide. Such effects are better bio-availability and reduced risk of side effects. An insidious disease, in treatment of which those particles can be utilized, is cancer.[8]

In this thesis, three different polyelectrolytes were studied with three different molecular weights. The pH-responsive behaviour was studied in three different pH conditions. The methods used for characterization and description of interesting behaviour were light scattering, specifically dynamic and static light scattering, measurements of zeta potential combined with potentiometric titration and small angle X-ray scattering, where the measurements were carried out in Biocev, Vestec.

This thesis is a part of long-term interdisciplinary research of Soft Matter group, which consists of primary synthesis of polyelectrolytes, characterization, self-assembly, tests of bio-compatibility and much more. One of the polyelectrolytes tested in this thesis was previously studied in the form of block A in amphiphilic block copolymers AB, AC or ABC.[6][9][10] However, so far the influence of molar mass and pH on the behavior of the polyelectrolyte block itself has not been studied.

1 Literature overview

1.1 Polyelectrolytes

Special type of macromolecules – polymers, which carry charged groups (and they are ionizable), are called polyelectrolytes (PEs). These ionisable groups could be negatively or positively charged after dissociation in polar solvents.[11] PEs, which contain strong acid or base groups, are called strong and PEs, which contain weak acid or base groups, are called weak. Those PE are described by their degree of ionization, which is defined as a fraction of the number of all dissociated groups to the sum of all dissociated and undissociated groups. A simple overview of PEs is shown in Figure 1.1.

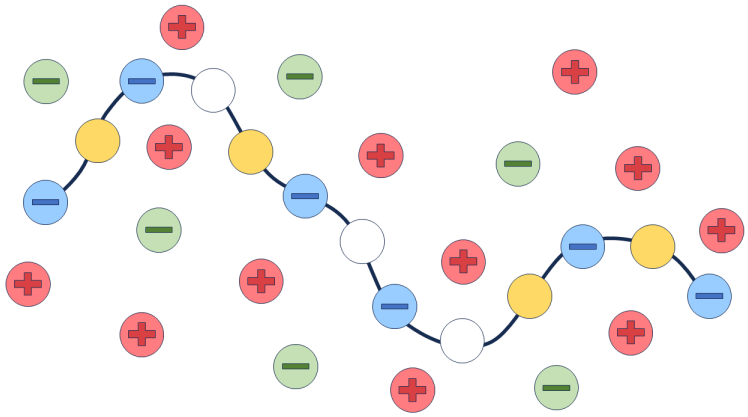

Figure 1.1 Schematic representation of PE chain (specifically polyanion) in solution in presence of additional salt. PE chain contains monomeric units with ionized groups (blue circles), non-ionized groups (yellow) and without ionizable groups (white). There are displayed counterions of PE (pink) and anions from added salt (green). Molecules of solvent are not included, because of clarity.

For description of PE behaviour, it is important to mention Coulomb law, which defines electrostatic energy U. The interplay of electrostatic energy U and thermal energy k_BT is the main reason for the presence of special PE properties.

$$U = \frac{q_1 q_2}{4\pi\epsilon\epsilon_0 r} \tag{1.1}$$

The influence of electrostatic energy U is dependent on distance between each charges. The distance at which the electrostatic interaction between two elementary charges e is equal to the thermal energy k_BT is defined as Bjerrum length.[11] [12]

$$\lambda_B = \frac{e^2}{4\pi\epsilon\epsilon_0 k_B T} \tag{1.2}$$

When the distance between two charged species is greater than the Bjerrum length λ_B, electrostatic interactions are weak and the thermal energy k_BT is dominant. For a smaller distance than the Bjerrum length λ_B, electrostatic interactions are dominant.

Because solutions of PEs have to be electroneutral, their charged groups are paired with counterions which, as mentioned before, dissociate in polar solvents. These solutions can be prepared with the defined ionic strength of the solvent and PEs are ionic-strength dependent. The influence of ionic stength is seen in conformations and intermolecular interactions of PEs. Subclasses of PEs behave slightly differently, for example polyanions or polycations form expanded structures in low ionic strength solutions. On the other hand, polyampholytes (PAs), which are described later, generally form shrunken structures, which decrease in size in low ionic strength solutions.[13] Additionally, as a result, the hydrodynamic radius can be tuned by different counterions.[14] If PEs are dissolved in solutions with finite salt concentrations, the electrostatic interactions between charged moieties are screened by salt ions. Moreover, some PEs require salt for dissolution.[11] Generally, in the solution with added salt, we cannot distinguish which ion belongs to the ionisable group of PE or has been in the solution before dissolution of the studied PE.

PEs and counterions in solutions are attracted towards each other and as a result, counterion condensation is promoted. It happens because of electrostatic attractions between opposite charges and the loss of the translational entropy, which is decreased when counterions and polymer chains are in the vicinity. However, in very dilute solution, the situation is different, because the entropic penalty is high and it is more efficient for counterions to stay "free" in solution.[11]

PEs are sensitive for pH alternation and it influences physical state and chemical structure. They can receive or release protons, so they undergo ionization and it increases surface charge of polymeric chain. Polyacidic chains are expanded, when pH of the solvent is greater than the pK_A value and oppositely, while pH of solvent is lower than the pK_A value, the chain length is decreased. Although, the polybase chain length is decreased while the pH of solvent is greater than pK_B and chain is expanded when the pH of solvent is lower than pK_B.[5] PE gels, which are a three-dimensional porous network structure, are also sensitive for pH alternations. Swelling occurs because of internal electrostatic repulsion in PEs with a net non-diffusible electric charge.[15] Degree of swelling (or absorption capacity AC) is a value, which defines how much liquid can be absorbed.

$$AC = \frac{(m_2 - m_1)}{m_1} \times 100\% \tag{1.3}$$

Where m_1 is weight of the PEs before swelling and m_2 is weight of the PEs after swelling.[16]

PEs' conformation is closely related to the number of ionized groups, because electrostatic interactions which promote PE chains shrinkage. There are several types of PE chain conformations: coil, sausage-like aggregate, necklace globule, spherical globule, and fully stretched chain. Conformation is also dependent on charge of the polymer. When the polymer is highly charged, the same charged groups repeal each other, then the chain expands, and a rod-like conformation is formed. The weakly charged polymer behaves differently. There is a smaller number of charged groups, they do not repel as much as in highly charged polymers. They tend to shrink and this conformation is called Gaussian coil.[11]

Compared to uncharged polymers, PEs behave differently in many ways. The viscosity of an uncharged polymers is proportional to the concentration of the

polymer.

$$\eta \sim c \tag{1.4}$$

While for PEs the Fuoss law applies, which says that the viscosity of the PE solution is proportional to the square root of the PE concentration.[17]

$$\eta \sim \sqrt{c} \tag{1.5}$$

Moreover, the osmotic pressure of salt-free PE solutions is greater than the osmotic pressure of analogous uncharged polymers. As osmotic pressure is one of the colligative properties, it depends only on the number of molecules present in a solution. PE solutions contain polymer chains as well as numerous counterions in comparison with the solutions of uncharged polymers, which contain only polymer chains. Therefore, the total number of molecules in a PE solution is much higher, so osmotic pressure of PE solutions is greater. The difference between a homogeneous solution of PEs and uncharged polymers is also seen by light scattering because of the peak which is only seen in PE solutions. The wave vector magnitude interrelated to this peak rises with $\sqrt{c}$. The transition from a dilute solution to a semi-dilute solution occurs at significantly lower polymer concentrations compared to those of solutions containing neutral chains. In the semi-dilute regime, PE chains follow unentangled dynamics across a broader concentration range, with the transition to entangled dynamics occurring at concentrations beyond those where uncharged polymers would typically overlap.[18][19][20] These solutions and also concentrated solutions are displayed in Figure 1.2.

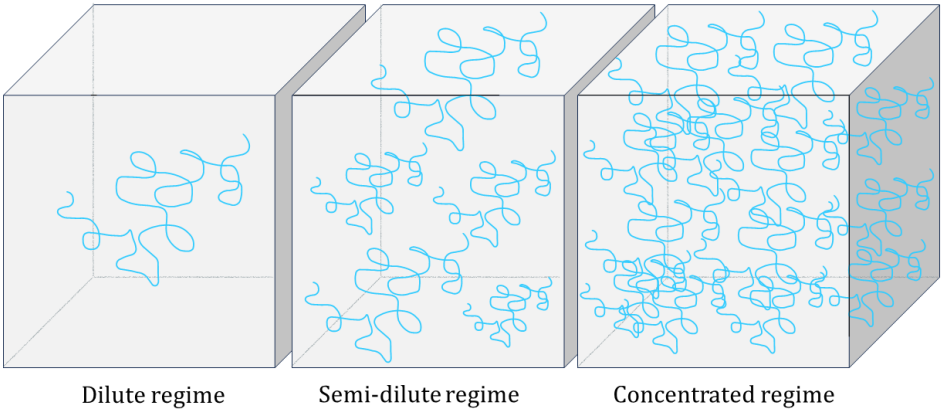

Figure 1.2 Representation of different concentration regimes of polymer solutions.

For understanding the Figure 1.2, we should define the segment concentration of a flexible chain as c (we can also name it the number of segments) and the segment concentration as a function of spatial distance $c(x)$. In dilute solutions, $c(x)$ has discrete values because the chains are distant. A lot of fluctuations are seen in semi-dilute regime, while in concentrated regime the values are not fluctuating, so they are continuous. When the concentration is increasing from the dilute regime to the semi-dilute regime, polymer chains are not as distant as

before and start to crossover, but in some regions it happens more extensively and in others less. Hence, fluctuations are observed. Lastly, in concentrated regime, crossing over the chains becomes uniform and the solution is evenly filled by polymer chains.[21]

Generally, PEs can be classified as weak or strong PEs - Figure 1.3. *Poly(acrylic acid)* is a weak polyelecrolyte, because it can not bear negative charge in wider range of pH values. *Poly(N-butyl-4-vinyl-pyridinium)* and *poly(styrene sulfonic acid)* are strong polyelectrolytes, because they bear charge in wide range of pH. Moreover, the first of them has a permanent positive charge, which is seen because of structure regardless of pH or other properties.

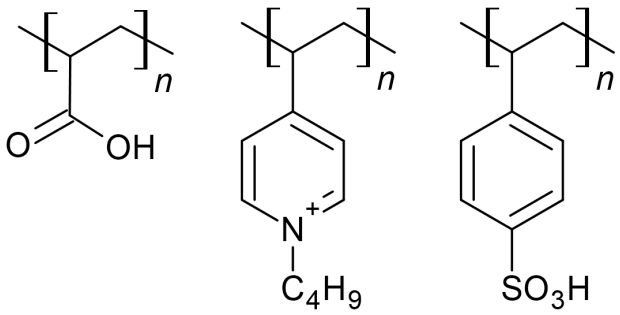

Figure 1.3 Examples of strong and weak PEs. From left to right: *poly(acrylic acid)*, *poly(N-butyl-4-vinyl-pyridinium)* and *poly(styrene sulfonic acid)*. To simplify the presentation counterions are omitted.

For a weak PE, it is specific that it can be reformed to an uncharged polymer by acidic or basic titration. Weak PEs, such as poly(methacrulic acid), do not have a charge at low pH. However, as the pH increases, it gains a negative charge. One of the first titrations of polyacids (specifically poly(methacrylic acid)) was performed by Katchalsky and Spitnik.[22] They found out that the titration curve of the polyacid is not the same as the ideal titration curve, which is described by Hendersson-Hasselbalch equation. Low molecular compounds typically behave in accordance to the ideal titration curve.

$$\mathrm{pH} = \mathrm{p}K_\mathrm{A} + \log \frac{\alpha}{1-\alpha} \tag{1.6}$$

They were working with the weak PE, for which ionization is suppressed in comparison with the low molecular compounds. Ionization costs extra free energy when neighbouring groups are ionized. Hence, other groups are not so willing to ionize because of electrostatic repulsion between the ionized species. It is harder to overcome the energetic barrier due to the extra energy cost and the titration curve becomes less steep. But as the number of charged groups increases, the repulsion between dissociated groups arises. This cause polymer chains to stretch during titration, which helps charged groups to move further apart and thus reduces electrostatic repulsion. In this case, work is being done against entropy, therefore, titration is connected with disadvantageous interactions, which increase the free energy of the chain by the enthalpy contribution.

On the other hand, strong PEs behave differently. They are charged at all pH values; therefore, have a permanent charge, which cannot be removed. Examples are polystyrene sulfonic acid and poly(allylaminehydrochloride).[23] [24] The

equilibrium state of strong PEs is established quickly, allowing us to consider their degree of ionization as a constant. By contrast, weak PEs are much more dependent on the pH of solution, and we cannot say that their degree of ionisation is a constant.

Another important attribute of PEs is the charge density, which is the amount of electric charge Q per unit volume, surface area or length. Biological molecule, which has the highest negative charge is heparin. It is commonly used as an anticoagulant.[25] Charge density is an important factor, which affects several non-negligible properties, such as absorption of PEs to specific surfaces (which could be used in the cosmetic industry [26]) and conformation after absorption and also degree of swelling of PEs could be tuned by that.[27]

Finer division of PEs consists of polyanions, polycations, PAs, and polyzwitterions (PZs). Examples of different types of PEs are shown in Figure 1.4. The subclass PE belongs to it is seen after dissociation and charged species are displayed.[1]

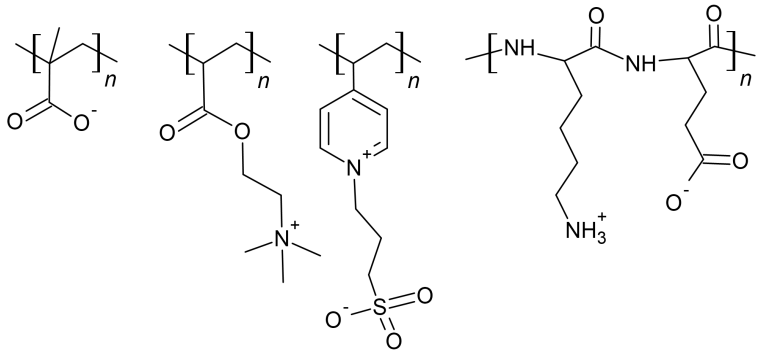

Figure 1.4 Examples of different types of PEs. From left to right: *poly*(*methacrylic acid*) - polyanion, *poly*[*trimethyl*(*2-*(*acryloyloxy*)*ethyl*)*ammonium*] - polycation, *poly*(*N-*(*propyl-3-sulfonate*)*-4-vinyl-pyridinium*) - PZ and *poly*(L-*lysine*-L-*co-glutamic acid*) - PA. To simplify the presentation counterions are omitted.

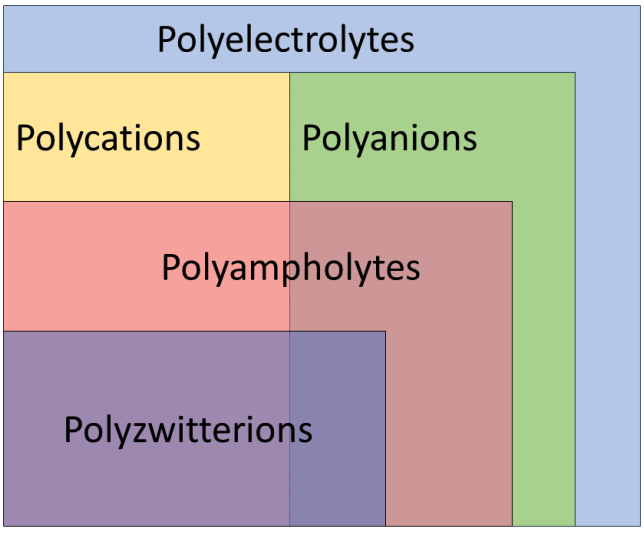

Figure 1.5 Schematic diagram, which displays relationships between each type of PE.

Figure 1.5 shows schematic relationships between each type of PEs. PAs are polymers that are made up of both positively and negatively charged monomer units. Therefore, the monomeric units contain positively or negatively charged groups and generally these monomer units alternate in the polymer chain.[28] Typically, PAs have a non-zero net charge because some of the charged species could be present only in a small pH window, apart from the narrow pH range, where the number of oppositely charged species may be equal. Moreover, the number of positively and negatively charged units may not be the same. Hence, their behaviour is mostly polycationic or polyanionic and is sensitive to pH and ionic strength.[29] PZs are polymers made of repeating units which contain pairs of oppositely charged groups and are classified as a subclass of PAs. They have overall neutral charge as they contain an equal number of positive and negative charges. Another synonymous name for PZs is polybetaines.[29][30] PZ's behaviour is dominated by strong Coulomb interactions, which cause high hydrophilicity.[31] Although PZs do not exhibit typical PE effects and share similarities with polar non-ionic polymers.[32] So, the difference between PZs and PAs lies in the positioning of charged species. Potential distributions of charged species in PZs are displayed in Figure 1.6 .

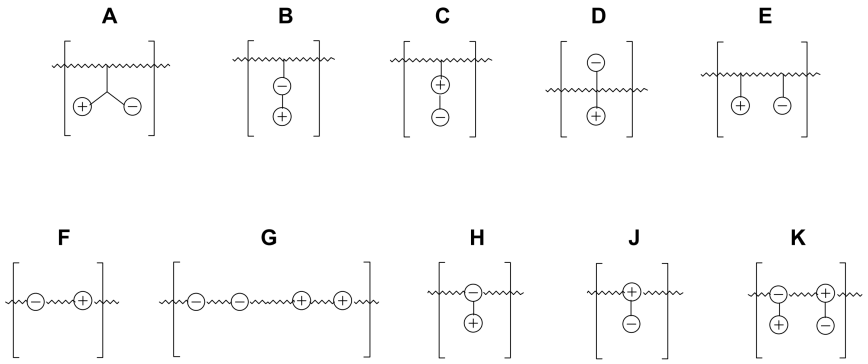

Figure 1.6 Potential distribution of ionic groups in PZs.[29]

So far, all architectures, except architecture *K*, have been synthesised.[32][33] Regardless, the most prevalent architecture is *C*. Typically, for synthesis, it is easier to implement the zwitterionic group into the side chain as are seen in architectures *A*-*E*.[29]

Overall, as a subgroup of PEs, PZs and PAs offer promising applications in biomedicine such as tissue engineering, drug delivery, implants, biosensors, antibacterial coatings or contact lenses.[28][30]

1.1.1 Block polyelectrolytes

Block PEs are a subcategory of block copolymers, which are formed by covalent binding of at least two different polymers. Overall, amphiphilic block copolymers can form various structures such as bilayers, vesicles, numerous types of micelles, and many more. These structures are self-assembled and there are numerous factors, which trigger this process, such as for example the type of solvent chosen, hydrophobicity, molecular weight, chain length, thermo/light/enzyme/pH-responsivity, etc. Block copolymers that respond to physical or chemical stimuli

are called stimuli-responsive and they could be used as smart materials.[34]

The block PEs by themselves combine several structural characteristics, which are seen in PEs, block copolymers, and also surfactants.

Typically, amphiphilic block PEs self-assemble into micelles, however, by changing the molecular weight of blocks, different architectures can be achieved, such as bilayers.[35] In case of micelles, the hydrophobic blocks form the core of the micelle, which is covered by the charged PE chains creating the shell or corona of the micelle. Formation of micelles is also influenced by the choice of solvent. One component of a micelle can be dissolved in specific solvents, which are called selective solvents.

1.1.2 Brief look at synthesis of polyelectrolytes

The synthesis of PEs is not an easy task and comes with many difficulties. Overall, it is often complex and requires multiple steps. The problem is that procedures, which can be applied for different substances, cannot be applied for PEs. They are often incompatible with numerous chemical reactions, because of the presence of charged species – electrophiles or nucleophiles (or even both of them). To avoid these unpredictable chemical conditions, ionic moieties could be added in post-polymerization process, however this approach does not solve the problem with direct methods of obtaining PEs.

Direct path of synthetising PZs from zwitterionic monomers by chain growth polymerization is often done by free radical polymerization.[32][36] This method has several advantages including tolerance of radicals towards both nucleophiles and electrophiles. Step growth polymerisation methods are used just occasionally.[29] The revolutionary technique for PE synthesis is controlled free radical polymerisation, where the growth of free radicals is in dynamic equilibrium with different types of dormant species and as results are narrow dispersity, the risk of branching is minimised and control over the architecture is secured. The useful features of this approach are the possibility of synthesis in aqueous solutions and no need to use post-polymerisation steps for introducing charged groups. An unusual method, which can be used for the synthesis of polymers, is utilisation of click reactions. It is a pathway which combines a wide range of advantages such as mild and simple reaction conditions, high yields, etc. Other widely used methods are nitroxide mediated polymerization (NMP), reversible addition fragmentation chain transfer polymerization (RAFT) and atom transfer radical polymerization (ATRP).[37][30][38] A frequent issue during synthesis is that salts are connected to charged groups and cumbersome work-up procedures are required for removing these ions. This is especially important for PZs.[29]

1.2 Characterization methods

This sections is devoted to description of the fundamentals of used characterization methods.

1.2.1 Light scattering

The interest in light scattering (LS) techniques originates from fact, that it is possible to determine molecular weight (because it is proportional in some manner to the scattering intensity) or other interaction parameters for solutions with either single or multicompoment solvents with them.[23] LS techniques are based on the phenomenon of the light interacting with a particle. The main interactions include absorption, scattering and a third interaction, which induces the constitution of charges in the particle, resulting in the formation of dipoles. Those dipoles emit electromagnetic radiation with specific frequency. If the frequency of the scattered light is the same as the initial, it is elastic scattering. On the contrary, when the frequency is changed, the process is called inelastic scattering. Moreover, another type of scattering is quasi elastic light scattering. In this case, the frequency of scattered light is almost the same as the frequency of the initial light. This type of scattering represents processes, where the frequency of initial light is alternated by the movement of the particles, which is called Doppler shift in wavelength. A technique related to these processes is called dynamic light scattering (DLS), which will be discussed later.[39][40]

Other scattering phenomena - reflection, diffraction and refraction appear in highly ordered systems. Here, we focus on scattering in solution, where particles are in constant free movement caused by Brownian motion. Hence, the system is highly unordered. The interference pattern of light depends on the size of the particles, as displayed in Figure 1.7. Accordingly, the interference can be constructive or destructive.[39][40]

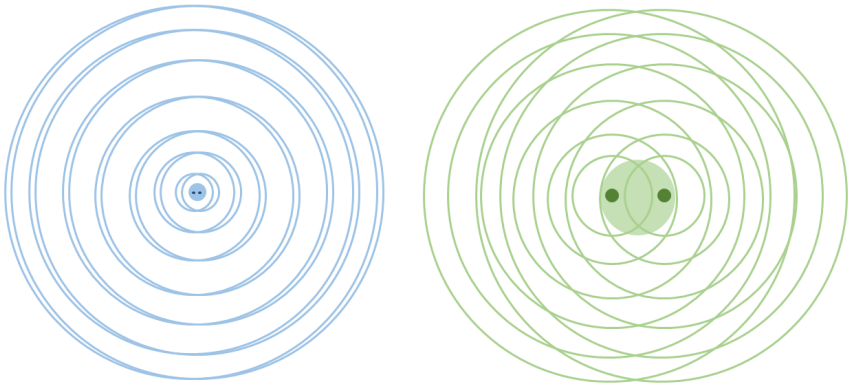

Figure 1.7 Interference pattern of the light scattered by small particles (left) and by large particles (right).

While the light passes through a solution, its intensity gets smaller by either scattering or absorption. The intensity of light scattered by a small molecule is defined as

$$I(r) = I_0 \frac{\pi^2 \alpha^2}{r^2 \lambda^4} \tag{1.7}$$

I_0 is the intensity of incoming light, α is the polarisability of the molecule, r is the molecule-detector distance and λ is the wavelength.[39] The intensity of scattered light is inversely proportional to λ^4, which implies that the blue light is scattered more than red light. Hence, this is a reason why the sky is blue or why milk is white.

Two complementary LS techniques are static light scattering (SLS) and DLS, where SLS measures the mean intensity of the scattered light, whereas DLS focuses on the fluctuations of the intensity of the scattered light (Figure 1.8).

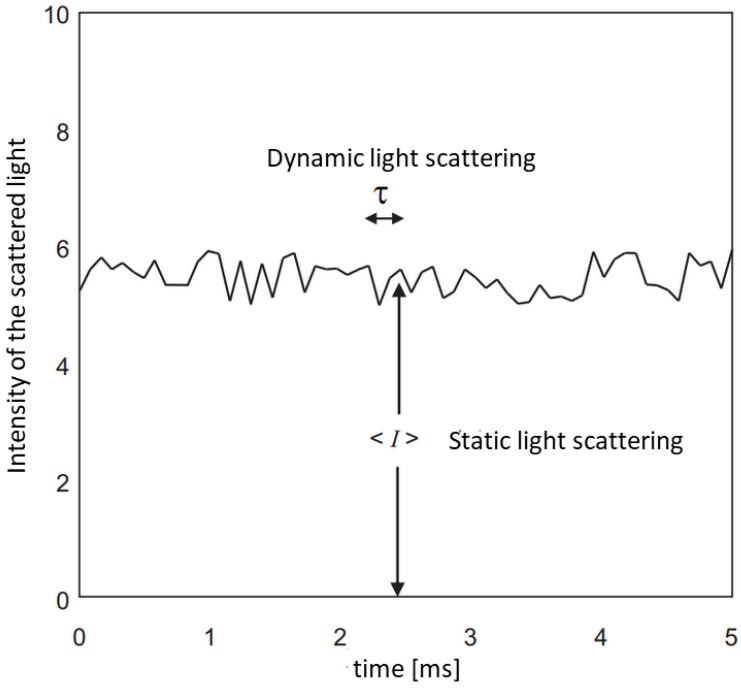

Figure 1.8 Comparison of the principles of static and dynamic light scattering.[39]

Static light scattering

SLS measures the intensity of scattered light at various angles (so the intensity depends on the observation angle θ) and the intensity values are time-averaged.[41] The molar mass of the scattering particles can be obtained from the averaged intensity. A more suitable quantity for the theoretical description of SLS is scattering vector $\vec{q}$, which is defined as the change in the wavevector, specifically a difference between the scattered wave vector $\vec{k_{out}}$ and the incident wave vector $\vec{k_{in}}$.

$$\vec{q} = \vec{k_{out}} - \vec{k_{in}} \tag{1.8}$$

The length of scattering vector can be expressed as

$$q = \frac{4\pi n}{\lambda_0} \sin \frac{\theta}{2} \tag{1.9}$$

n is the refractive index of the medium, λ_0 is the wavelength of the light in vacuum. Figure 1.9 displays how the direction of the wavevector changes because of the collision of the incident light with the scattering particle.

Figure 1.10 displays how the observational length scale depends on the magnitude of scattering vector. With bigger q values, more sample details are observed. It can be compared with inverse microscopy - when q values are small, the magnification and with that corresponding resolution is lower.[40]

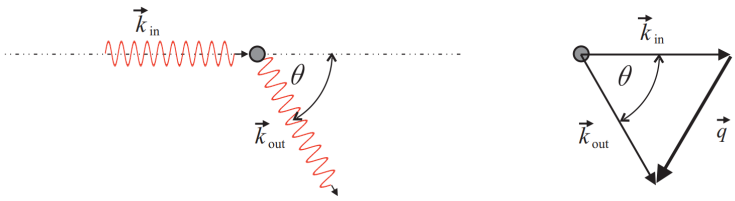

Figure 1.9 Change of the wavevector due to the collision with the scattering particle (left) and vector representation (right).[39]

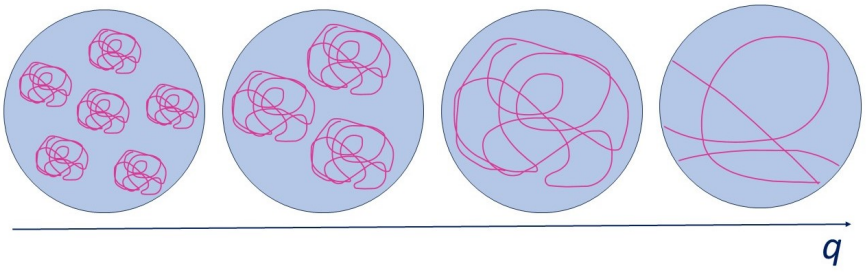

Figure 1.10 Details observed in a sample containing polymer coils on q-scale.

For actual measurements, it is important that the absolute scattering intensity depends only on the system properties, which can be defined by the Rayleigh ratio as a function of q,

$$R(q,c) = \frac{I_s(q)r^2}{I_0 V_s(q)} \tag{1.10}$$

$I_s(q)$ is the intensity of the scattered light as a function of q, r is the distance scattering volume - detector, I_0 is the initial intensity of the laser and $V_s(q)$ is the scattering volume, which is the volume illuminated by laser and simultaneously seen by the detector.

The information about molecular weight and size of the particles can be obtained from multi-angle SLS measurements. The corresponding equation is the Zimm equation

$$\frac{Kc}{R(q)} = \frac{1}{M_w}(1 + \frac{1}{3}q^2R_g^2) + 2A_2c + ... \tag{1.11}$$

where c is the concentration, R_g is the radius of gyration, A_2 is second virial coefficient, which defines attractive and repulsive forces between particles. K is the optical contrast constant and it is defined as

$$K = \frac{4\pi^2 n_0^2 (dn/dc)^2}{N_A \lambda_0^4} \tag{1.12}$$

N_A is Avogadro constant and dn/dc is a refractive index increment, which represents the change of the refractive index with the change of the concentration and it is important quantity for determination of weight concentration.[39]

To obtain the molecular weight, the second virial coefficient and the radius of gyration, it is necessary to perform multi-angle measurements of a series of solutions at different concentrations and construct a Zimm diagram. The intercept of the plotted data extrapolated to zero angle and zero concentration gives the

reciprocal of M_w, while slope of the scattering intensity at the extrapolation to $q = 0$ provides the value of A_2 and the slope of the extrapolation to $c = 0$ yields the information about R_g.[41]

Other possibility of size determination is via Guinier plot, which is characterized by equation 1.13. It is also used as an intermediate step for molecular weight determination of large particles.[39]

$$\ln I_s(q) = \ln I_s(0) - \frac{1}{3}q^2 R_g^2 \tag{1.13}$$

Dynamic light scattering

DLS measures the fluctuations during short time periods, which allows us to determine the diffusion coefficient D of macromolecules.[41] The fluctuations in the scattered intensity are a direct consequence of the movement of scattering particles, known as Brownian motion. This movement stems from the random thermal density fluctuations of the solvent molecules. Moreover, the Brownian motion of charged particles can be affected by presence of charges due to the attractive or repulsive forces, which can accelerate or slow down the motion.[8] The diffusion coefficient is defined by the Stokes-Einstein equation.

$$D = \frac{k_B T}{6\pi\eta R_h} \tag{1.14}$$

k_B is the Boltzmann constant, T is a temperature, η is a solvent viscosity.[40] R_h is the hydrodynamic radius, which relates to the radius of the hypothetical hard sphere with the same speed of diffusion as the particle of the interest.[42]

The correlation function indicates the relative motion of particles with use of means of an electric field correlation function.[43] At short time intervals, the correlation is high, because the particles do not have enough time to move significantly. So, they can be considered static. However, when the time interval is longer, the correlation decreases exponentially, because the initial and final state are different.

The function, which describes motion of investigated particles is called an intensity correlation function. Normalised intensity correlation function is defined as

$$g_2(\tau) = \frac{\langle I(t)I(t+\tau)\rangle}{\langle I(t)\rangle^2} \tag{1.15}$$

τ is the lag time between the two time points.

The electric field correlation function describe the motion of particles relatively to each other. The normalised form is defined as

$$g_1(\tau) = \frac{\langle E^*(t)E(t+\tau)\rangle}{\langle I(t)\rangle} \tag{1.16}$$

These two correlation functions can be coupled in one equation, which is called the Siegert relation and is defined as

$$g_2(\tau) = B + \beta|g_1(\tau)|^2 \tag{1.17}$$

B is the baseline, which is approximately 1 and β is the correction factor, which is dependent on the instrument and scattering properties of the studied particles.[43]

The data obtained by DLS measurements need to be fitted to provide the diffusion coefficient and other quantities, which are related to it. First method is the cumulant method, which is composed from two cumulants. Second order cumulant expansion is defined as

$$\ln g_1(\tau, q) = -\Gamma_1 \tau + \frac{\Gamma_2 \tau^2}{2} \tag{1.18}$$

First cumulant Γ_1 provides information about the average diffusion coefficient and is defined as

$$\Gamma_1 = q^2 \langle D \rangle \tag{1.19}$$

The equation 1.19 is related to the diffusion coefficient, which can be used to determine the hydrodynamic radius by Stokes-Einstein equation (1.14).

The second cumulant Γ_2, which is defined as

$$\Gamma_2 = (\langle D^2 \rangle - \langle D \rangle^2) q^4 \tag{1.20}$$

and provides information about dispersity of the diffusion coefficient distribution function.[44][40][45] The data, which are obtained experimentally, are apparent diffusion coefficients. To obtain the true values of diffusion coefficients is needed to extrapolate data to zero concentration and zero angle.

Second and one of the most popular data analysis method is constrained regularization method for inverting data (CONTIN). This method utilizes Laplace transform and nonlinear statistical techniques. This technique is more suitable for disperse systems.[43] It provides the distribution of relaxation times $A(\tau)$ by the inverse Laplace transform applied on correlation function $g_1(t)$.[45]

$$g_1(t) = \int_0^\infty A(\tau) \exp\left(-\frac{t}{\tau}\right) d\tau \tag{1.21}$$

CONTIN contributes good estimates for the data with good signal to noise.[46]

The topology of the scattering particle can be derived from the particle size provided from SLS - R_g and from the particle sizes provided from DLS - R_h. It can be defined by the ρ-ratio, which is expressed as

$$\rho = \frac{R_g}{R_h} \tag{1.22}$$

For homogeneous sphere is the value of the ρ-ratio 0.775 and for hollow sphere is the value 1. Other theoretically calculated values are available in the literature.[40]

1.2.2 Small angle X-ray scattering

Small angle light scattering is a robust analytical technique, which can help with sample characterization in various fields, such as materials science, structural biology or generally environmental sciences.[47] Other techniques, which can complement small angle x-ray scattering are x-ray crystallography, NMR, circular dischroism, DLS or fluorescence. Information about the size, shape, pore size, the radius of gyration or even distribution of macromolecules can be earned from

small angle scattering measurements.[48] Importantly, this technique provides averaged information about whole system from all electron scatterings.[49] The angles, which are typical for small angle scattering, range from 0.1° to 5° parallel to the plane of scattering.[48] Measured samples, placed in quartz capillary, can be illuminated by X-rays - small angle X-ray scattering (SAXS), which are scattered by atomic electron shell or by neutrons - small angle neutron scattering (SANS), they are scattered by atomic nuclei.

X-ray beam has a specific energy, which is inversely proportionate to the wave length λ.

$$E = \frac{hc}{\lambda}$$

For anode sources, the wave length is fixed. Hence, it cannot be tuned. For synchrotron sources, the wave length may be tuned. The X-ray scattering by electrons of atoms ordered in a crystalline lattice with the spacing d follows the Bragg equation.[50][48]

$$n\lambda = 2dsin(\theta) \tag{1.23}$$

Subsequent quantities are present in are present in the equation - θ as scattering angle, d as interplanar d-spacing, λ as wavelength of used beam source and n as diffraction order. Intensity of scattered rays needs to be recorded - it is possible via an x-ray detector. For further investigation and data analysis is needed to measure the pure solvent intensity, which is referred to as a buffer. Afterwards, it is subtracted from the sample scattering intensity, which leads to the clear signal made from the interested particles as is shown in Figure 1.11.[49]

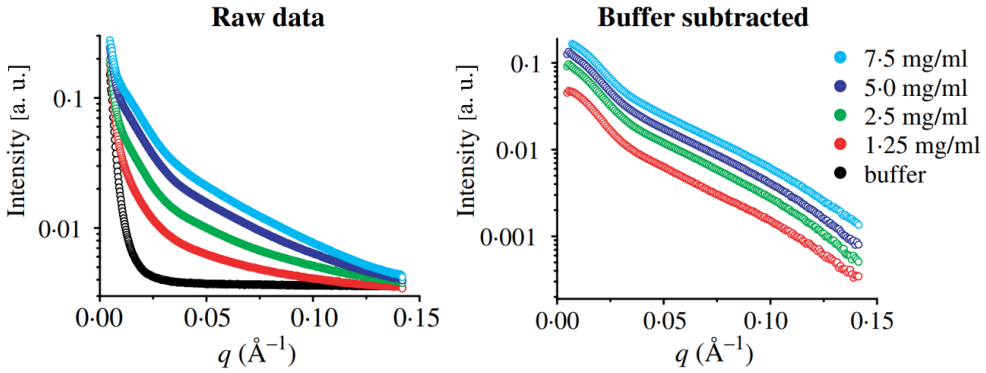

Figure 1.11 Representation of raw SAXS data and buffer subtracted data and intensity dependence on concentration.[51]

The crucial step is to correctly match the buffer to the corresponding sample. SAXS is a sensitive method, hence even small discrepancies can make big impact in context of buffers, but also the purity of samples. The scattering intensity of the sample is proportional to the concentration - if the concentration is higher, the signal-to-noise ratio of subtracted data will be better. From steepness of intensity at low angles is usually possible to tell, whether the sample is aggregating. When the intensity is decreasing, repulsive inter-particle interactions are present. However, when the intensity sharply increases, it may represent unspecific aggregation of the sample.[50][49] Polymeric systems often have quite low contrast in

the SAXS measurements, reason for that is a not big difference in the number of electrons in subsequent atoms - N, C, O and H. In small angle neutron scattering, the contrast can be tuned by heavier atoms, for example deuterated solvents or partially deuterating some components can help with studying each components of system separately. Hence, it obtains more detailed structural information due to the highlighting some parts of system. However, in SAXS measurements, this is not possible, because the electron density of H and D is the same.[52]

The scattering curves obtained from experimental measurements display dependence of scattering intensity I on q, which is a scattering vector. The double logarithmic scale is commonly used, since, the details at the large q values are highlighted. To achieve desired structure information, it is needed to nonlinearly fit the scattering data with various models. The obtained curves are composed from three regions of q-s: high q, middle q also called Porod and low q region also called Guinier region. The Guinier region provides the radius of gyration R_g, obtained from the Guinier equation (equation 1.13).

R_g is defined as

$$R_g^2 = \frac{\int_V \rho_e(\mathbf{r})|\mathbf{r}|^2 dV}{\int_V \rho_e(\mathbf{r}) dV} \tag{1.24}$$

Middle q region provides information about the shape of studied particles, which is determined by the slope of the scattering curve characterized by power law exponent α, when the intensity $I(q)$ pursue a power law:

$$I(q) \propto q^{-\alpha} \tag{1.25}$$

Power-law scattering is present in samples with some kind of morphology, for example porous structures. Overall, it originates from the surface with roughness, however, it can also come from the dispersity of the sample. Power-law exponent is associated with the fractal dimension D. The idea of fractal dimension comes from concept, that this one number can describe a very complex roughness. The power laws connected to SAXS curves can come from mass fractals ($D_m < 3$), where the roughness is present in bulk volume, and surface fractals ($D_s < 3$, $D_m = 3$), where the roughness is located at the surface. Typical values of the power-law exponent values are in the range $0 < \alpha \leq 4$.[47]

Information about inner structure of particles is provided by high q regions.

The scattering pattern in small angle scattering is composed from two contributions. First of them is called the form factor $P(q)$, which comes from the shape of the particle and pore size, thus we can say, it is a consequence of intraparticle interference. And second of them is called the structure factor $S(q)$, which comes from the composition of particles or pores. In such manner, we can say, it is a consequence of interparticle interference. The structure factor is dependent on the concentration of scattering particles. Charged macromolecules or generally charged nanoparticles structure factor is present as sharp maximum. The shape determination of the particles is often impeded by polyelectrolyte effect. In this case, addition of salt helps with the reduction of charges. For more concentrated and disperse systems, it is not possible to describe interactions with just one structure factor, because of interactions of all particles between each other. Hence, for these type of systems is needed to utilize more complicated fits and establish various approximations.[47]

1.2.3 Zeta potential

A physical property that showcases any macromolecule or generally a particle in suspension is zeta potential (ZP). It could be especially helpful for optimalization of formulations of protein solutions, suspensions or emulsions because of determining stability.[53][54]

The particles in dispersion may adhere to each other and form aggregates. Size of these particles is decreased in comparison to particles by themselves and they may settle out because of gravity influence. Firstly formed aggregate is called a floc and the its formation process is called flocculation. A floc might sediment or phase separate, but it might also remain stable. Another important process is coagulation, which happens when the aggregate transforms imto a much denser form and then usually separates out by sedimentation as shown in Figure 1.12. The important difference between coagulation and flocculation is that, in general, coagulations cannot be reversed, whereas flocculation is reversible.[55]

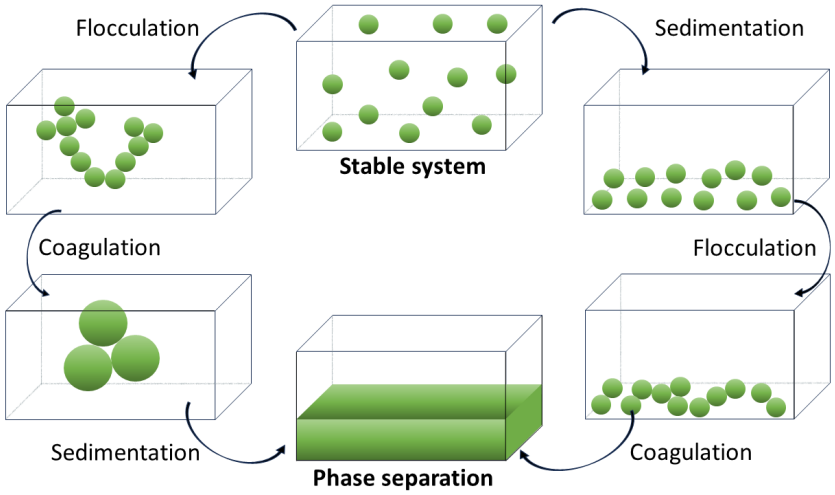

Figure 1.12 Schematic diagram of processes which may occur in colloidal dispersion where stability might be missed.

The sum of van der Waals attractive and electrical double layer repulsive forces determines the stability of a colloidal system. These forces interact, when the particles come in contact with each other, because of the Brownian motion. At first, repulsive forces prevent the particles from mutual contact however, when they gain enough energy (by for example an increase in temperature), they are able to overcome this barrier and subsequently attractive forces bind the particles strongly and irreversibly. As long as the repulsive forces are dominant, the colloidal system is stable. The stability could be obtained in two ways. Firstly, we can introduce a layer of polymer coating, which prevents particles from coming into the close contact. These coatings keep particles separated by steric repulsion and van der Waals forces are not strong enough. Secondly, electrostatic or charge stabilization regulates interactions.[55]

As seen in Figure 1.13, the particle is surrounded by the liquid layer, which consists of two parts, the inner region (also called the Stern layer) and the outer (or difuse region). In the Stern layer the ions are bound to the surface of a colloidal particle and in the diffuse region, as the name implies, the particles are less densed.

The barrier formed by these ions from the bulk dispersant is called the slipping plane. The electrical potential of this barrier is known as ZP.[53]

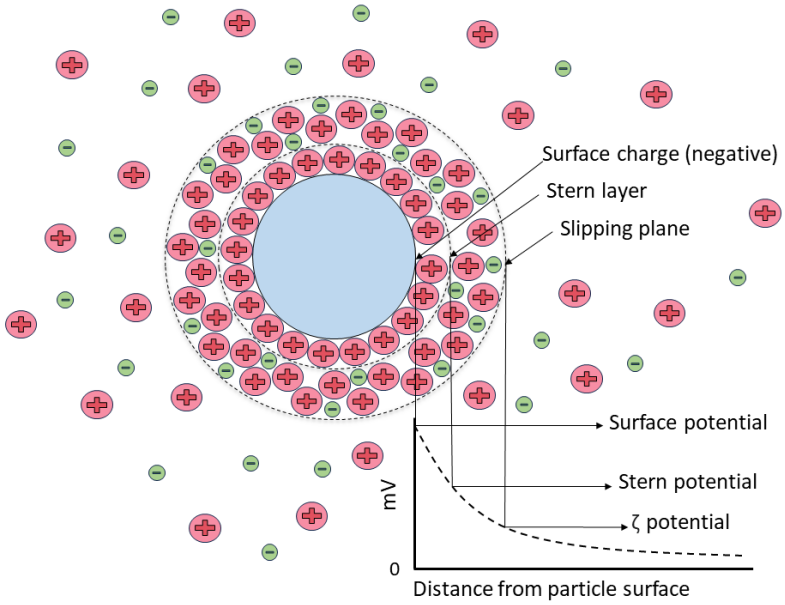

Figure 1.13 Schematic representation of zeta potential.

Generally, it is said that the suspensions are stable, when their ZP values are more positive than +30 mV or more negative than -30 mV.[53] The reason for this comes from the assumption that when the particles have a large ZP (negative or positive), they tend to repel each other and they cannot flocculate.[54]

ZP can be affected by several factors. The most important being the pH of aqueous solutions. ZP can vary as pH changes. Important state which occurs at zero ZP, associated with specific pH values is the isoelectric point.[44]

The existence of charges on the surface of a particle causes a response to applied electric field. The responses to the electric field are called electrokinetic effects, which include electrophoresis, electroosmosis, streaming potential and sedemimentation potential. For us, the most important is electrophoresis which is a process of when particles with charged species are attracted towards the oppositely charged electrode. This movement is opposed by viscous forces. When these two forces reach equilibrium, the particles move with constant velocity. ZP comes out in the Henry equation, which defines electrophoretic mobility U_E.

$$U_E = \frac{2\epsilon\zeta f(\kappa a)}{3\eta} \tag{1.26}$$

κ is called Debye length and it refers to the "thickness" of the electrical double layer and the parameter a is the radius of the particle. $f(\kappa a)$ is a number and if it is related to aqueous medium and moderate concentration of electrolyte or PE, its value is 1.5 and it is called the Smoluchowski approximation. ϵ is a dielectric constant and η is a viscosity.[55]

2 Aim of the thesis

The main goal of this thesis is to investigate the self-assembly behavior of newly synthesized PEs in aqueous solutions by scattering techniques. The study focuses on how molar mass and ionization states at different pH values affect the structural and dynamic properties of the PE solutions. These solutions are examined at constant ionic strength and in the dilute region. Techniques used include static and dynamic light scattering (SLS) and (DLS), small-angle X-ray scattering (SAXS), and zeta potential measurements. The polyelectrolytes analyzed are poly((sulfamate-carboxylate)isoprene) (PISC), poly((amino-carboxylate)isoprene) (PACIS) and poly((trimethylammonium-carboxylate)isoprene) (qPACIS) in three molecular weights - 7.5, 38 and 75.5 kDa.

The specific aims were:

1. To characterize PISC, PACIS and qPACIS solutions with different molecular weights in three different pH conditions using LS measurements containing SLS and DLS.

2. To study size and structure of PISC, PACIS and qPACIS aggregates with different molecular weights in solution in three different pH conditions using SAXS.

3. To measure zeta potential ζ of PACIS, PISC and qPACIS solutions with different molecular weights in pH spectrum ranging from 1 to 12.

3 Materials and used methods

3.1 Studied polyelectrolytes

PE samples analysed in this thesis were synthesised by Ing. Katarzyna Byś (Soft Matter Group, the Department of Physical and Macromolecular Chemistry, Charles University). Specifically, they are poly((amino-carboxylate)isoprene) (PACIS), poly((sulfamate-carboxylate)isoprene) (PISC) and poly((trimethylammonium-carboxylate)isoprene) (qPACIS). Both PACIS and PISC were synthesised from purchased cis-1,4-polyisoprene (PIS) (M_W = 7.5 kDa, $Đ$ = 1.04, Polymer Source Inc., Canada) and PIS (M_W = 75.5 kDa, $Đ$ = 1.08, Polymer Source Inc., Canada) (these polymers were prepared via anionic polymerization) and from purchased PIS (average $M_W \sim 38$ kDa by GPC, made from natural rubber, SigmaAldrich, United States). qPACIS was synthesised from the same PIS from natural rubber source.

Synthesis of all three PEs (PISC, PACIS and qPACIS) begins with a starting polymer PIS, which undergoes the post polymerization modification of its C=C double bonds in reaction with chlorosulfonyl isocyanate. The synthetic pathway is seen in Fig. 3.1.

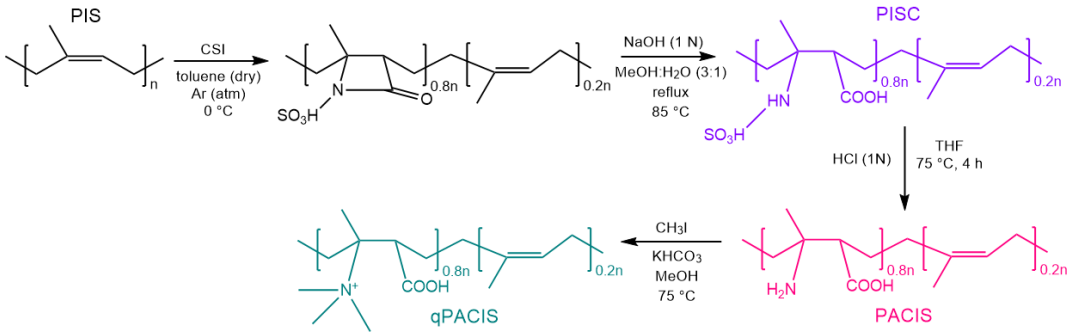

Figure 3.1 Synthetic pathway of studied PE. To simplify the presentation counterions are omitted.

The lactam intermediate is formed, which needs to be hydrolysed in alkaline conditions using NaOH. The reaction mixture needs to be dialysed in consequence of excess NaOH used for hydrolysis. The dialysis was carried out against double distilled water with use of dialysis membranes with molecular weight cut-off 3500 Da, until the pH of the dialysis bath was neutral. The aqueous solution acquired from dialysis was lyophilized, which provided final product - PISC. To achieve polyzwitterionic PACIS, it is needed to continue with acid-induced cleveage, which cleaves N-S bonds of the sulfonyl groups. After acid treatment, dialysis against 0.1 M HCl is required. As before, the aqueous solution acquired from dialysis was lyophilized, which provided final product - PACIS. The quaternization of the amine groups of PACIS leads to qPACIS, which was carried out by quaternizing agent CH_3I in presence of $KHCO_3$. The unreacted CH_3I was washed out from the solution with chloroform. Unwanted reaction of a free carboxyl group and CH_3I can lead to an ester, due to this reason, it is needed to use 0.1 M HCl. As before, the final product was achieved after dialysis against double distilled water and

lyophilization. The same procedures were carried out for all three used molecular weights of PISs.

3.2 Sample preparation

All samples for LS and SAXS were prepared by dissolving the solid polymer samples in three different pH conditions, in 0.1 M DCl (A), 0.1 M NaCl in D_2O (N) and 0.1 M NaOD (B). The 0.1 M DCl solution was made by using 20 wt. % DCl and D_2O and in the similar way, the solution of 0.1 M NaOD was made by using 30 wt. % NaOD and D_2O. Used deuterated solvents were: DCl (20 wt. % in D_2O, 99.5 at. % D, Chemontrade, Germany), D_2O (99.9 % D, SigmaAldrich, United States) and NaOD (30 wt. % in D_2O, 99 at. % D, SigmaAldrich, United States). For samples in 0.1 M NaCl in D_2O was used NaCl from Lach-Ner (Czech Republic). Deuterated solvents were used due to the previous preparation of samples for NMR DOSY measurements, where they are required.

The concentration of samples for LS was 1 mg/ml and for SAXS was 5 mg/ml. Every sample and solvent were filtrated though 0.2 μm membrane filter using a 1 ml syringe before the measurements. Samples of a volume around 1 ml for LS were directly filtered to pre-cleaned and dusted with a compressed air glass tubes, which were closed up with rubber top.

The samples for ZP were prepared at the initial concentration 1 mg/ml. Used PEs were dissolved in 0.1 M HCl, which was prepared from ampoule for preparation of 0.1 M 1000 ml volumetric solution (P-LAB, Czech Republic). pH of samples was adjusted using 0.1 M NaOH on the titrator. Solution of NaOH was prepared from ampoule for preparation of 0.1 M 1000 ml volumetric solution (P-LAB, Czech Republic). Used water for all procedures was purified by Barnstead MicroPure water purification system (Thermo Scientific, United States).

3.3 Instrument specifications

3.3.1 Light scattering

The light scattering measurements (DLS and SLS) were carried out simultaneously on ALV light scattering photometer (ALV, Germany). The photometer is equipped with ALV CGS - 3 automatic goniometer, an ALV 7004 Multiple-Tau digital correlator, a Cobolt Flamenco diode-pumped solid state laser ($\lambda = 660$ nm, $P = 100$ mW) (Hübner Photonics, Germany), two high-QE avalanche photodiodes pseudo cross-correlation detectors (Excelitas Technologies, USA). The measurements were operated via ALV-Correlator Software V.3.0.

All measurements were performed for the scattering angles starting from 50° to 130° with angular step of 10°, at temperature 23 °C. The instrument is equipped with a cell housing system containing toulene, which is used as an index matching fluid, before measurements is needed pre-calibration for the toluene standard. Whereas, all samples were prepared with deuterated solvents, pre-recorded D_2O file was used for all measurements, as well as file with the toluene standard.

3.3.2 SAXS

SAXS measurements were carried out in the BIOCEV centre (Vestec, Czech republic) on a SAXSpoint 2.0 (Anton Paar, Austria). This instrument is equipped with a MetalJetC2+ X-ray source containing a liquid gallium alloy anode ($\lambda = 0.134$ nm) and with an EIGER R 1M Horizontal detector. Samples were loaded into 1 mm quartz capillary by high precision low volume auto-sampler with temperature control (which was set on 20.00 °C). The sample-to-detector distance was 0.78 m to which is corresponding the q vector range starting from 0.047 to 4.4 nm^{-1}. For obtaining SAXS curves is needed azimuthal averaging of scattering patterns, for both the samples and the buffers(in our case D_2O), and then subtracting buffers intensities from belonging samples intensities.

3.3.3 Zeta potential

pH adjustment was carried out on a Metrohm 888 Titrando Compact titrator equipped with a magnetic stirrer, a Pt1000 temperature sensor and for measuring pH was used a LL Biotrode 3.0 mm glass electrode. Titrando Software was used for collecting the results and for controlling the titrator.

ZP (ζ) measurements were carried out on Malvern Zetasizer Utra equipped with 633 nm He - Ne gas laser and with avalanche photodiode. Each sample was placed into standard polystyrene cuvette and dip cell was used. The obtained values of ζ-pontential were averaged from 3 subsequent measurements by the instrument. One measurement consisted maximally from 100 runs, the number of repeated runs was dependent on quality factor, which was evaluated automatically by the instrument. PISC NR and PACIS NR were measured once, but other samples were measured three times and averaged. ζ-pontential values were calculated from electrophoretic mobilities using the Henry equation in the Smoluchowski approximation, $\mu = \frac{\epsilon\zeta}{\eta}$, where μ is the electrophoretic mobility, η is the solvent viscosity and ϵ is the dielectric constant of the solvent.

4 Results and discussion

4.1 Ionic properties of studied polyelectrolytes

Used PE contain ionizable groups (weak acids or bases), which means their ionization state responds to pH changes of the environment. However, the ionization of weak PE is not as straightforward as for low molar mass molecules. It is generally known that an acid is almost fully ionized at pH $>$ pK_a + 1. Although, PE are 50% ionized at the maximum under these conditions. pH in the vicinity of PE chain, which is called local pH, can highly differ in comparison with pH measured by conventional pH-meter, which is called the bulk pH. Local pH describes local variations of pH, but they are difficult to measure. Bulk pH describes pH far from PE chains and influence them minimally.[56]

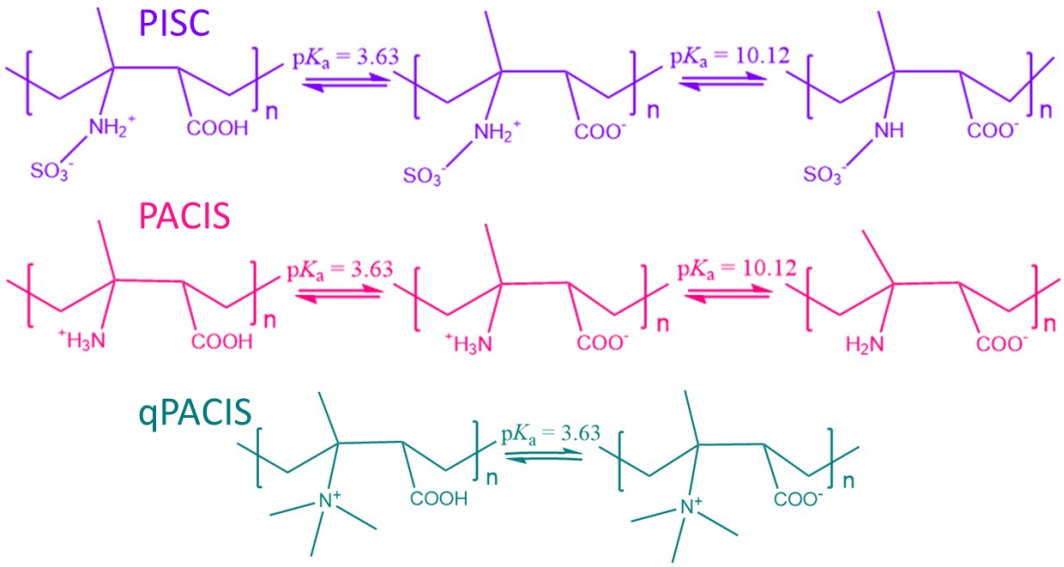

Figure 4.1 Ionization schemes with determined pK_a values of PISC, PACIS and qPACIS. To simplify the presentation counterions are omitted.

Determined pK_a values of carboxylic group and amino group were based on the molecular dynamics simulations for a low molecular compound resembling a monomeric unit of PACIS done by Pablo M. Blanco, Ph.D (Soft Matter Group, the Department of Physical and Macromolecular Chemistry, Charles University). The initial pK_a values needed for simulations, were estimated by Chemaxon pK_a predictor. pK_a value of carboxylic acid is 3.63, pK_a value amino group is 10.12 and pK_a value of sulfonic acid is smaller than 1, which means this group is always deprotonated due to our stated conditions.

Typically, the first estimated values of pK_a values of low molecular compounds, which resembles monomeric units of PEs, are good estimates for the initial values needed for the simulations. However, the pK_a values determined by the simulations can highly differ from the real pK_a values due to the inter and intramolecular interactions.

The counterion size plays major role in size of formed aggregates due to the counterion condensation, which helps to achieve more compact structures.[57]

Below the pH = 3.63 (pK_a of carboxylic group) and below pH = 10.12 (pK_a of amino group) both groups are ionized and charged oppositely, which is an important factor for solubility, because the neutralization of charges can lead to aggregation due to the instability of this state.

Importantly, studied PEs contain 20 % of unmodified monomeric units of the starting polymer PIS, which influences solubility (in terms of poorer solubility), because those parts are hydrophobic. Generally, PEs are water soluble. Moreover, hydrophobic domains influence ionization of PEs.

4.2 Associates size determination by dynamic and static light scattering measurements

The analysis of DLS measurements yields a distribution of the particle sizes, specifically hydrodynamic radius R_h shown as intensity weighted, mass weighted and number weighted. The distribution was calculated by the constrained regularization algorithm CONTIN (by using software Alv-Correlator V.3.0) at 90°. Since, the studied aggregates are not homogeneous spheres for which the form factor in CONTIN is defined, the mass and number weighted distributions of R_h might be prone to error. Solutions of three different pHs were compared for each measured PE.

SLS measurements were evaluated by plotting $\ln I(q)$ vs. $\ln q$ to obtain power law exponents α, $I(q) = Aq^{-\alpha}$, from the slopes. Scattering data with $\alpha < 1$ were fitted with the Guinier formula, $\ln I(q) = \ln I_0 - \frac{R_g^2 q^2}{3}$, to obtain gyration radius R_g, which can be found in Table 4.1.

Table 4.1 Radius of gyration R_g obtained from Guinier plots from the measurements at 90°

Polymer	$R_g[nm]$	Polymer	$R_g[nm]$
PISC 7k A	34	PACIS NR A	45
PISC 7k N	49	PACIS 75k A	52
PISC NR A	32	PACIS 75k N	57
PISC 75k A	25	PACIS 75k B	68
PISC 75k N	35		

The intensity weighted distributions functions of hydrodynamic radius R_h are displayed in Figure 4.2 A. Only PISC 7k N shows monomodal distribution with not completely separated peaks with mean peak size 15 nm. From distribution is visible that the scattering particles have two sizes, but majority of them has smaller size. Other two distributions are multimodal and contain one big peak with bigger size, especially PISC 7k B with 177 nm and second smaller peak has size 4 nm. PISC 7k A distribution shows small particles with size 0.58 nm and bigger particles with size 21 nm. In span of couple of days, it formed gel-like structure, which indicates the instability of the solution. It is caused due to the short chains of PISC 7k being rigid and constrained in regards to the

conformation. In the intensity weighted distributions, the bigger particles have bigger impact than small particles, because the bigger particles scatter a lot more. In mass weighted and number weighted distributions, those bigger peaks are not displayed or have smaller intensity compared with the peaks displayed in intensity weighted distributions. The mass weighted distribution of PISC 7k A shows major peak with size 0.6 nm and hardly visible peak with size 9 nm. The number weighted distribution confirms particle size 0.6 nm. PISC 7k N shows relatively broaden peak in mass weighted distribution with size 2 nm. The broaden peak was expected due to the broaden peak in the intensity weighted distribution. The number weighted distribution shows peak with smaller size 2 nm. PISC 7k B shows bimodal mass weighted distribution with sizes 1 and 4 nm. The number weighted distribution displays peaks with size 1 nm and size 4 nm, which is hardly visible.

The plot $\ln I(q)$ vs. $\ln q$ shows that PISC 7k A and PISC 7k N belong to the Guinier area, because their slopes are smaller than 1. Hence, their values of radius of gyration can be evaluated. PISC 7k B slope with value bigger than 2 shows that it forms enormous compact particles. The repulsion of individual chains plays role in the aggregation process. As, it can be seen in Figure 4.2 A, the distribution is multimodal, which is also important factor. Hence, the slope of the Guinier plot is bigger than 1, the dependence is subjected to the power law and does not belong to the Guinier area. The fit is not relevant for this particles, because its size exceeds the size threshold suitable for LS analysis. In this case, on LS scale, we can observe the inner structure of the particles. Moreover, the values of R_g can not be evaluated.

The intensity weighted distributions for PISC NR are displayed in Figure 4.3 A. PISC NR A has multimodal distribution, but first peak contributes by small fraction. The major peak has size 59 nm. This solution precipitated in span of one day. Only PISC NR N shows monomodal distribution with not completely separated peaks with mean peak size 96 nm. PISC NR B has multimodal distribution, but first peak contributed by small fraction. The major peak has size 160 nm.

Again, as before it is visible that the scattering particles, which were small and almost were not visible on the intensity weighted distribution are dominant on mass and number weighted distributions. PISC NR A shows on mass weighted distribution bimodal distribution with sizes 7 nm and 32 nm. PISC NR N (3 nm) and PISC NR B (4 nm) have monomodal mass weighted distributions.

PISC NR A number weighted distribution contain two peaks - first with size 7 nm and second, which is contribution by fraction of percent, with size 22 nm. PISC NR N and PISC NR B shows monomodal distributions with sizes 3 nm for N and 3 nm for B.

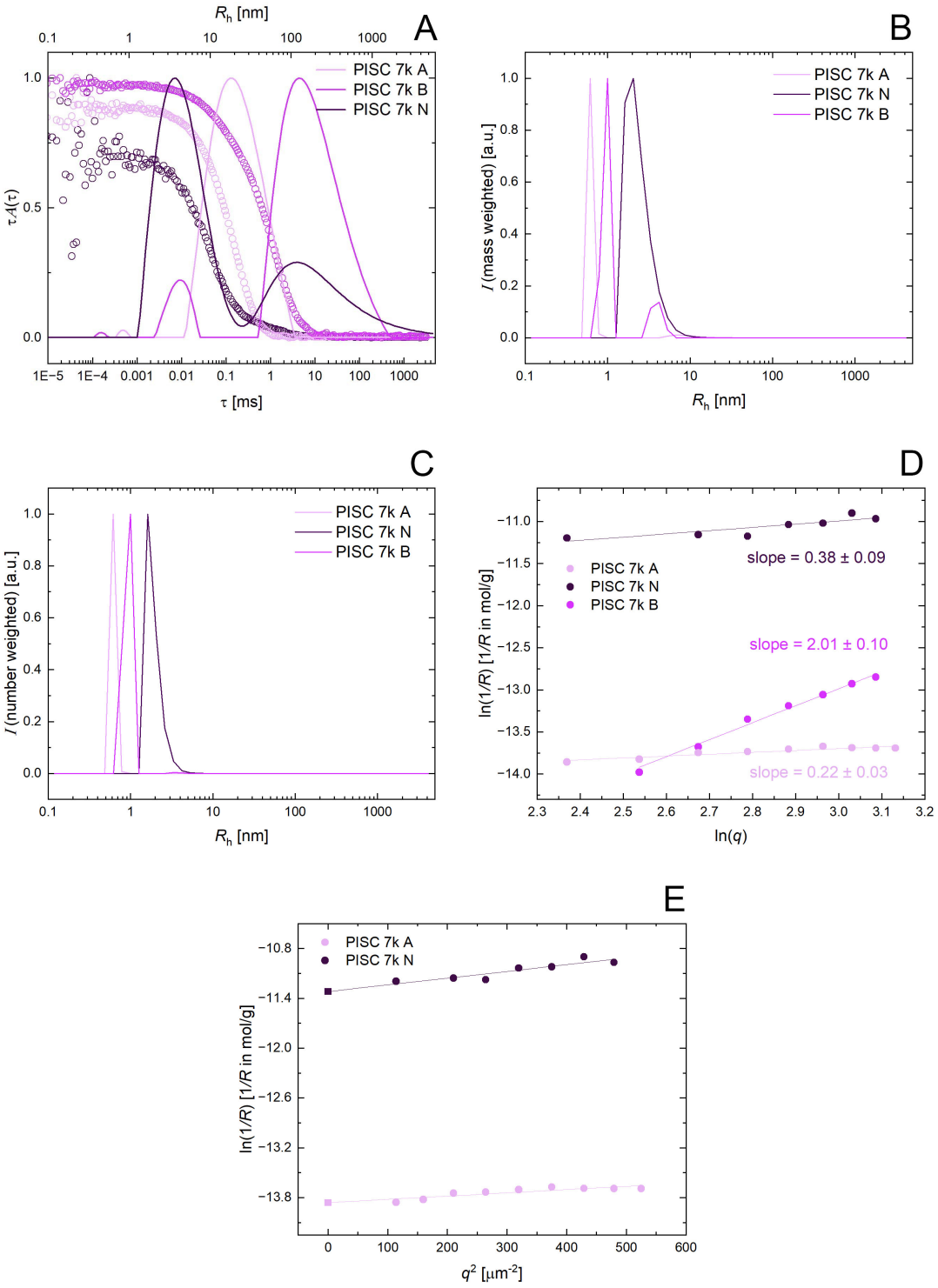

Figure 4.2 DLS correlation functions and intensity weighted (A), mass weighted (B), number weighted distribution functions of hydrodynamic radius R_h (C), plot $\ln I(q)$ vs. $\ln q$ (D) of PISC 7k in acidic (0.1 M DCl), neutral (0.1 M NaCl in D_2O) and basic (0.1 M NaOD) solution and Guinier plot of PISC 7k A and PISC 7k N (E). The error bars are not visible, their size is smaller than the size of the symbols. Square symbols symbolize the values extrapolated to zero angle and zero concentrations.

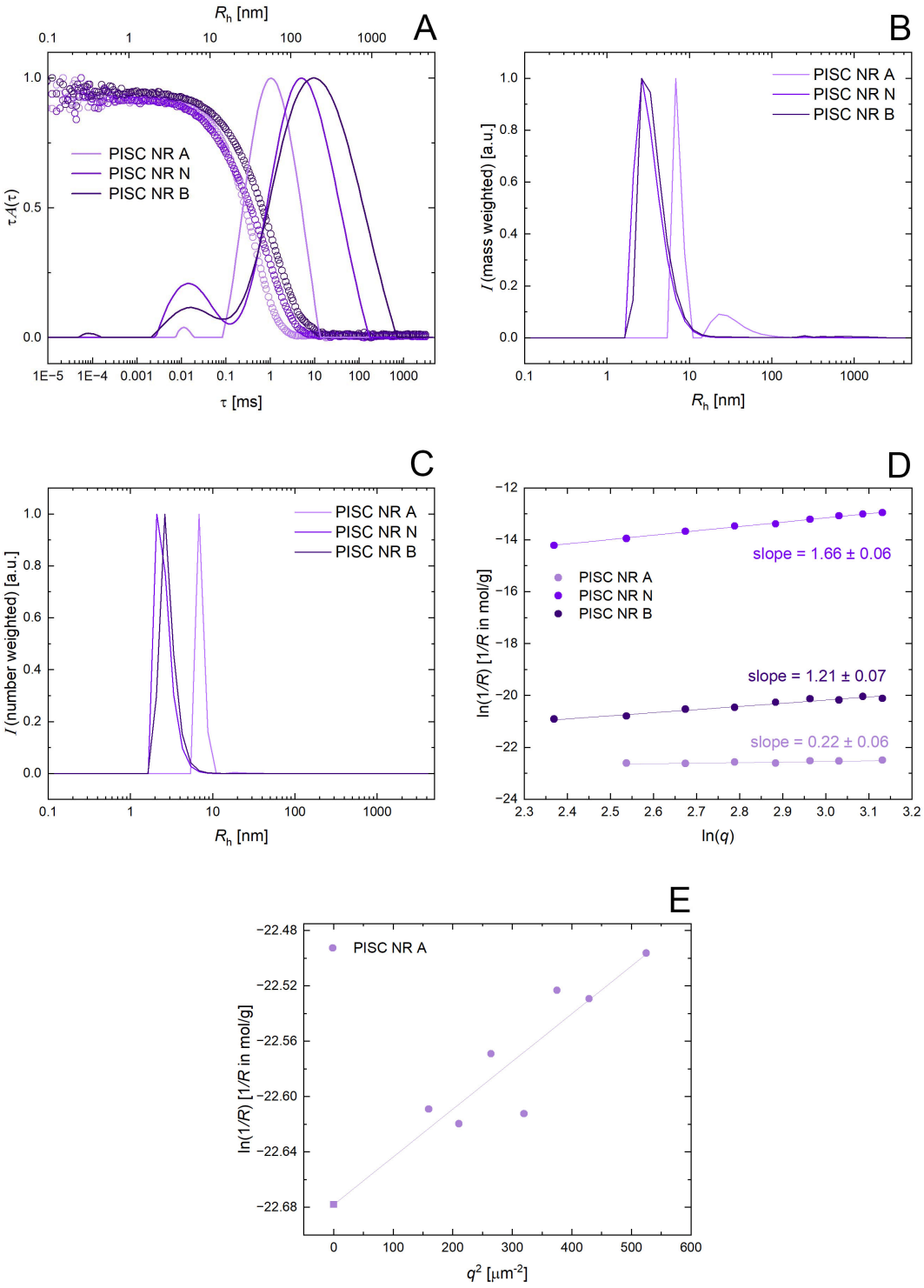

Figure 4.3 DLS correlation functions and intensity weighted (A), mass weighted (B), number weighted distribution functions of hydrodynamic radius R_h (C), plot $\ln I(q)$ vs. $\ln q$ (D) of PISC NR in acidic (0.1 M DCl), neutral (0.1 M NaCl in D_2O) and basic (0.1 M NaOD) solution and Guinier plot of PISC NR A (E). The error bars are not visible, their size is smaller than the size of the symbols. Square symbols symbolize the values extrapolated to zero angle and zero concentrations.

The plot $\ln I(q)$ vs. $\ln q$ shows that PISC NR A belong to the Guinier area. The slopes of PISC NR N and PISC NR B are bigger than 1, the dependencies have power law and does not belong to the Guinier area. The fits are not relevant for this particles, because of their large size. Moreover, the values of R_g can not be evaluated. Typical value 1.7 of the slope describes aggregates and the diffusion controlled aggregation. It is enough to touch for the individual particles to form an aggregate. Hence, the aggregates can resemble flakes and it could be said that the aggregate is composed from branches of individual aggregating particles. Therefore, the structure is not compact. However, as the value of slope increases up to two, the aggregate is more compact and repulsion starts to play important factor. Further increase of the slope value up to three means the aggregate is homogeneous, compact and does not scatter light. The light can be scattered by this kind of objects just because of different index of fraction.

The intensity weighted distributions of PISC 75k are displayed in Figure 4.4 A. PISC 75k A contains two peaks, but as before small peak contributes very little to the distribution. The major peak has size 17 nm. PISC 75k N distribution is monomodal, but this peak is broaden and its size is 15 nm. PISC 75k B distribution contains three peaks, but as before first is contributing very little. Two other peaks has size 6 nm and 381 nm, which is quite a large particle.

From mass weighted distributions is visible that PISC 75k A contain two sizes of particles with 1 nm and 8 nm. As in intensity weighted distribution, PISC 75k N peak in mass weighted distribution is broaden with size 3 nm. PISC 75k B distribution is bimodal and major peak is narrow and its size is 1 nm. Minor peak has size 5 nm.

The number weighted distributions are displayed in Figure 4.4 C. PISC 75k A contain contributions in this distribution, but second of them contribute. First major peak has size 1 nm and second peak has size 6 nm. PISC 75k N and PISC 75k B shows monomodal distribution. The size of PISC 75k N is 2 nm and PISC 75k B has size 1 nm.

Again, in mass weighted and number weighted distributions are not seen big scattering particles with tens of nanometers sizes, which means number of this scattering particles is small and can not be seen on other distributions, but the intensity weighted distributions show those particles due to the stronger scattering.

The plot $\ln I(q)$ vs. $\ln q$ shows that PISC 75k A and PISC 75k N belong to the Guinier area and their R_g can be evaluated. PISC 75k B slope value is bigger than 1, its R_g can not be evaluated due to the size, which exceeds the size threshold suitable for LS analysis and the fit is not relevant.

The intensity weighted distributions of PACIS 7k are displayed in Figure 4.5 A. PACIS 7k A have multimodal distribution and contain three peaks. The major peak is narrow and its size is 148 nm. First peak has size 4 nm and second peak has size 16 nm. The peaks are nicely separated. PACIS 7k N contains one peak, which is composed from two incompletely separated peaks. Its mean peak size is 55 nm. PACIS 7k B distribution contains two peaks, which the major of them is broaden, its size is 3 nm. First peaks size is 186 nm.

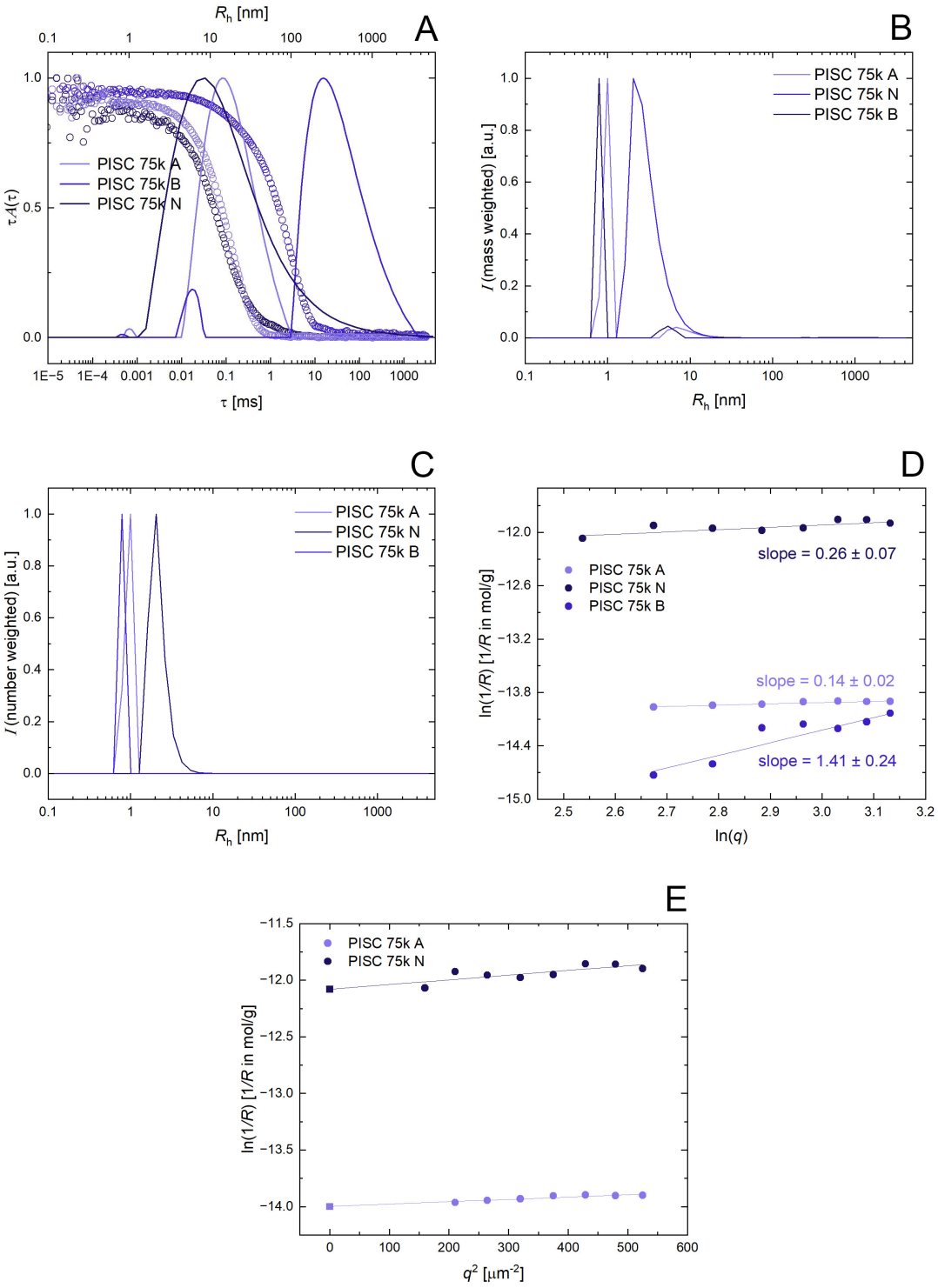

Figure 4.4 DLS correlation functions and intensity weighted (A), mass weighted (B), number weighted distribution functions of hydrodynamic radius R_h (C), plot $\ln I(q)$ vs. $\ln q$ (D) of PISC 75k in acidic (0.1 M DCl), neutral (0.1 M NaCl in D_2O) and basic (0.1 M NaOD) solution and Guinier plot of PISC 75k A and PISC 75k N (E). The error bars are not visible, their size is smaller than the size of the symbols. Square symbols symbolize the values extrapolated to zero angle and zero concentrations.

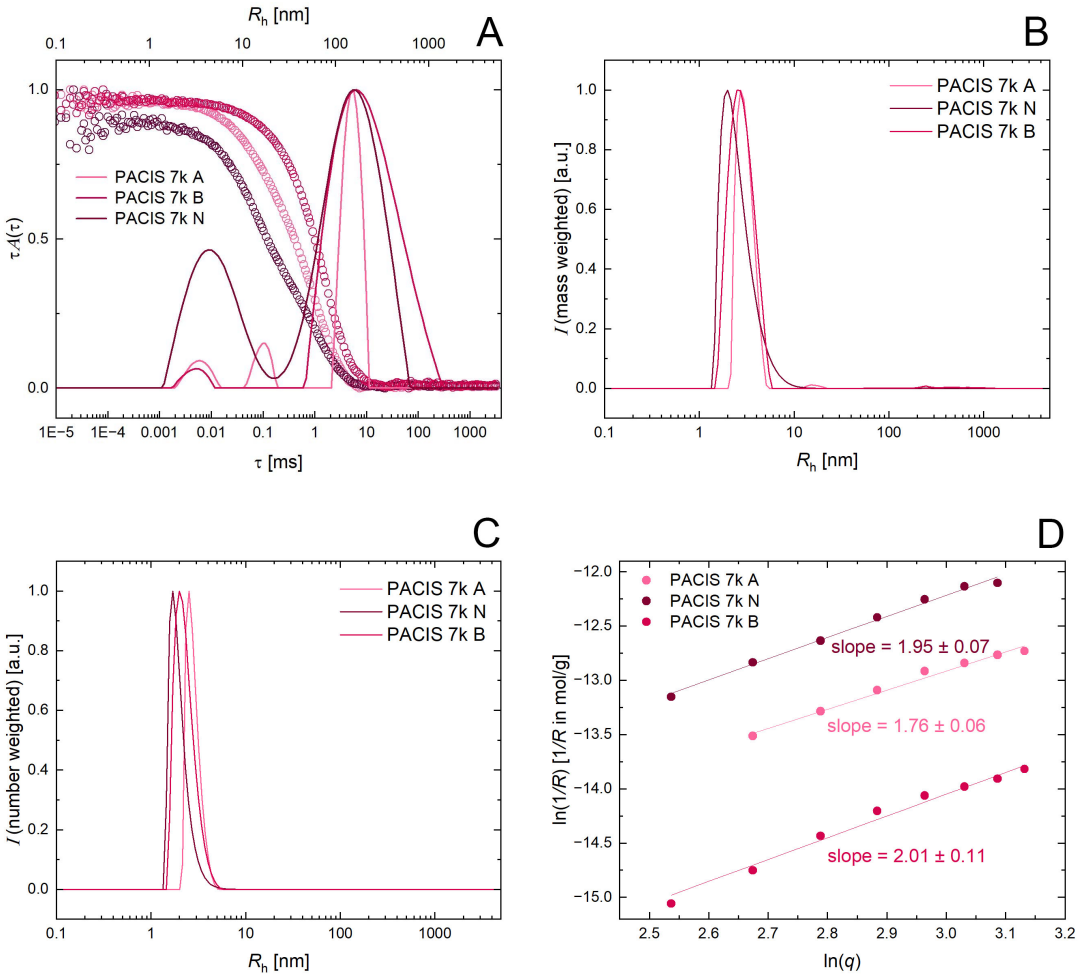

Figure 4.5 DLS correlation functions and intensity weighted (A), mass weighted (B), number weighted distribution functions of hydrodynamic radius R_h (C), plot $\ln I(q)$ vs. $\ln q$ (D) of PACIS 7k in acidic (0.1 M DCl), neutral (0.1 M NaCl in D_2O) and basic (0.1 M NaOD) solution. The error bars are not visible, their size is smaller than the size of the symbols. Square symbols symbolize the values extrapolated to zero angle and zero concentrations.

The mass weighted distribution of PACIS 7k A shows three peaks, but the second and the third are small and contribute minimally. The size of the first peak is 3 nm, the second is 15 nm and the third is 158 nm. The major peak is narrow. PACIS 7k N contains just one peak with size 3 nm. PACIS 7k B has broaden major peak and its size is 3 nm. The second peak, which contributes minimally has size 331 nm.

The number weighted distribution shows just one peak for all PEs. PACIS 7k A size is 3 nm. PACIS 7k N has size 2 nm. PACIS 7k B has size 2 nm.

The plot $\ln I(q)$ vs. $\ln q$ was made for all PACIS 7k solutions. For all applies, the dependence has power law and does not belong to the Guinier area. The fit is not relevant for this particles, because its sizes are so big. Moreover, the values of R_g can not be evaluated. PACIS 7k A has close values of slope (1.70), which describes diffusion controlled aggregation. PACIS 7k N and B are compact scattering particles. For PACIS 7k B can be seen inner structure in LS measurements.

The intensity weighted distributions of R_h for PACIS NR are displayed in Figure 4.6 A. PACIS NR A distribution contains just one peak, which is composed from two not completely separated. The size of this peak is 50.18 nm. For the reason that those peaks are not separated, the peak is wide. PACIS NR N contains two peaks, which are near each other. The first peak has size 5 nm and the second peak has size 171 nm. The distribution of PACIS NR B is multimodal and contains three peaks. All peaks are narrow. The major peak has size 424 nm, which is enormous size, here it has to be admitted, it could be some dirt or dust. Two other peaks are much smaller with sizes 4 nm and 55 nm.

The mass weighted distributions of PACIS NR can be found in Figure 4.6 B. PACIS NR A contains one peak, with relatively broad distribution in comparison with other peaks, which corresponds with the intensity weighted distribution. The size of this peak is 4 nm. PACIS NR N contains two peaks with size 4 nm and 191 nm. This sizes are relatively similar with the intensity weighted distribution. PACIS NR B contains three peaks (same as in the intensity weighted distribution). First two peaks are nicely visible with sizes 1 nm and 4 nm, but third contributes little to the distribution and it size is 451 nm.

The number weighted distributions shows that PACIS NR A is monomodal with size 3 nm and PACIS NR N and PACIS NR B are bimodal, but the contribution of second peak is small. PACIS NR N first peak has size 4 nm and second peak has size 29 nm. PACIS NR B first peak is 1 nm and second peak is 4 nm.

The plot $\ln I(q)$ vs. $\ln q$ shows that PACIS NR A belong to the Guinier area and the R_g values can be evaluated. The slope values of PACIS NR N and PACIS NR B are bigger than 1. Moreover, PACIS NR N value is bigger than 2. The dependencies have power law and do not belong to the Guinier area. The fits are not relevant for those particles, because the particle sizes are so big. Moreover, the values of R_g can not be evaluated. As the value of slope is 2, all scattering particles are compact and on LS scale is visible inner structure of aggregates.

The intensity weighted distributions of PACIS 75k are displayed in Figure 4.7 A. All distributions are monomodal and their peaks are composed from two peaks, which are not completely separated, just PACIS 75k B contains small peak, which contributes negligible. PACIS 75k A has size 30 nm, PACIS 75k N has size 27 nm and PACIS 75k B has size 29 nm. All peaks are broaden.

The mass weighted distributions are displayed in Figure 4.7 B. All distributions are monomodal. The size of PACIS 75k A is 3 nm. PACIS 75k N has size 3 nm and PACIS 75k B is 2 nm. The size obtained from this distributions are significantly different than from the intensity weighted distributions.

The number weighted distributions are similar to mass weighted distributions. Again, all distributions are monomodal and provide significantly smaller values. PACIS 75k A has size 3 nm. The size of PACIS 75k N is 2 nm. PACIS 75k B has size 2 nm.

The plot $\ln I(q)$ vs. $\ln q$ shows that all PACIS 75k belong to the Guinier area, because their slope values are smaller than 1. Hence, the values of R_g can be evaluated via Guinier plot.

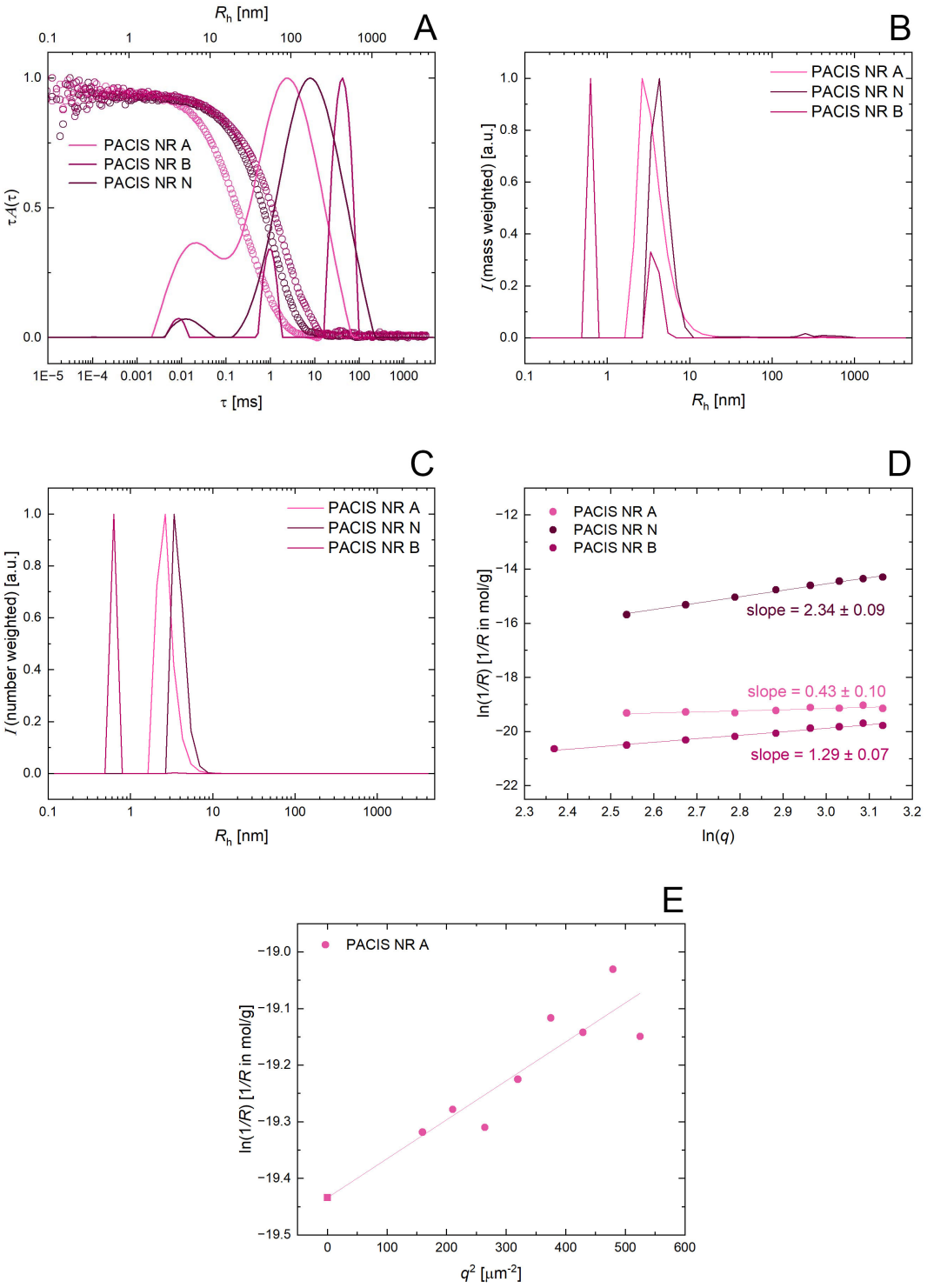

Figure 4.6 DLS correlation functions and intensity weighted (A), mass weighted (B), number weighted distribution functions of hydrodynamic radius R_h (C), plot $\ln I(q)$ vs. $\ln q$ (D) of PACIS NR in acidic (0.1 M DCl), neutral (0.1 M NaCl in D_2O) and basic (0.1 M NaOD) solution and Guinier plot of PACIS NR A (E). The error bars are not visible, their size is smaller than the size of the symbols. Square symbols symbolize the values extrapolated to zero angle and zero concentrations.

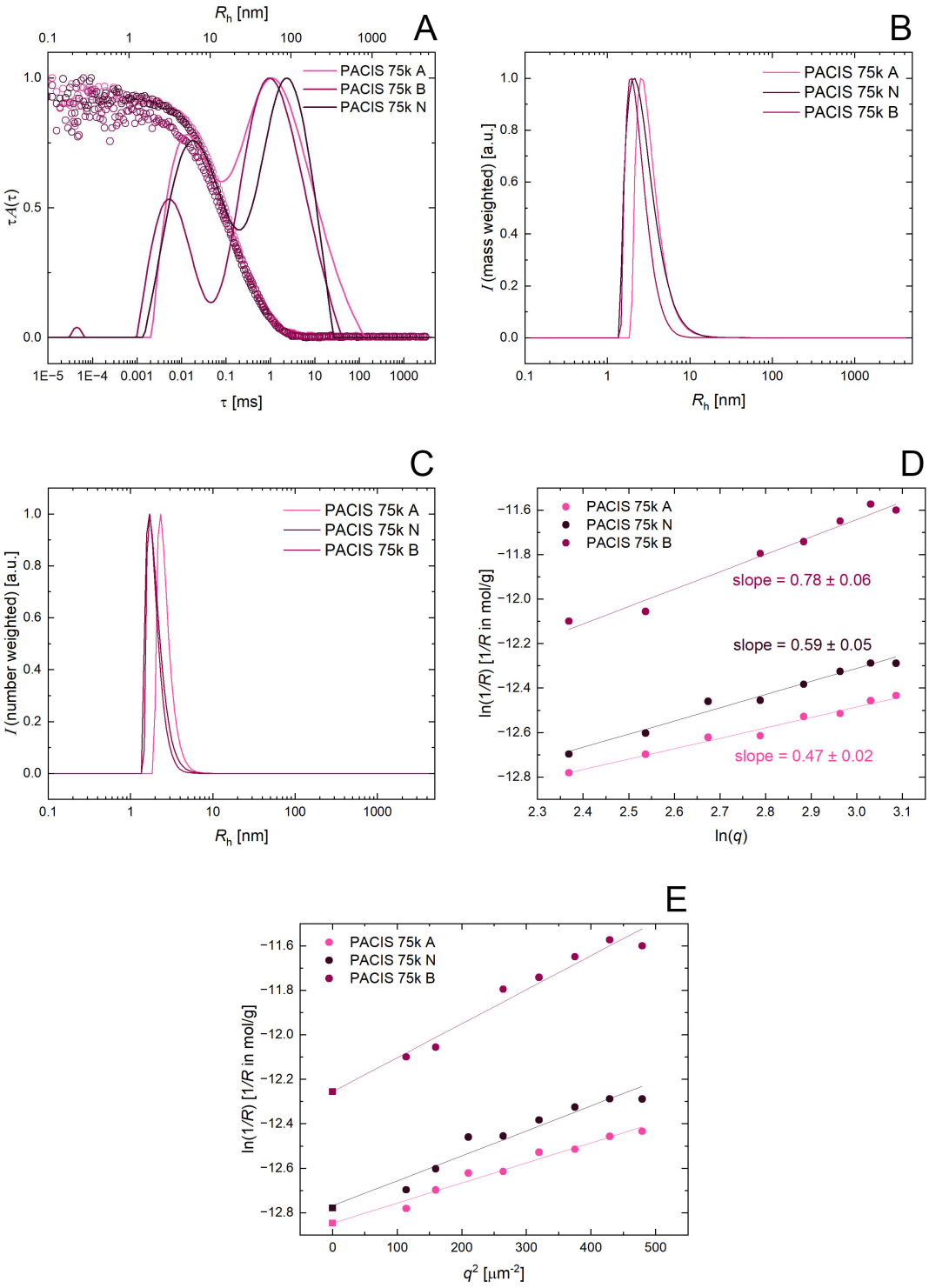

Figure 4.7 DLS correlation functions and intensity weighted (A), mass weighted (B), number weighted distribution functions of hydrodynamic radius R_h (C), plot $\ln I(q)$ vs. $\ln q$ (D) and Guinier plot (E) of PACIS 75k in acidic (0.1 M DCl), neutral (0.1 M NaCl in D_2O) and basic (0.1 M NaOD) solution. The error bars are not visible, their size is smaller than the size of the symbols. Square symbols symbolize the values extrapolated to zero angle and zero concentrations.

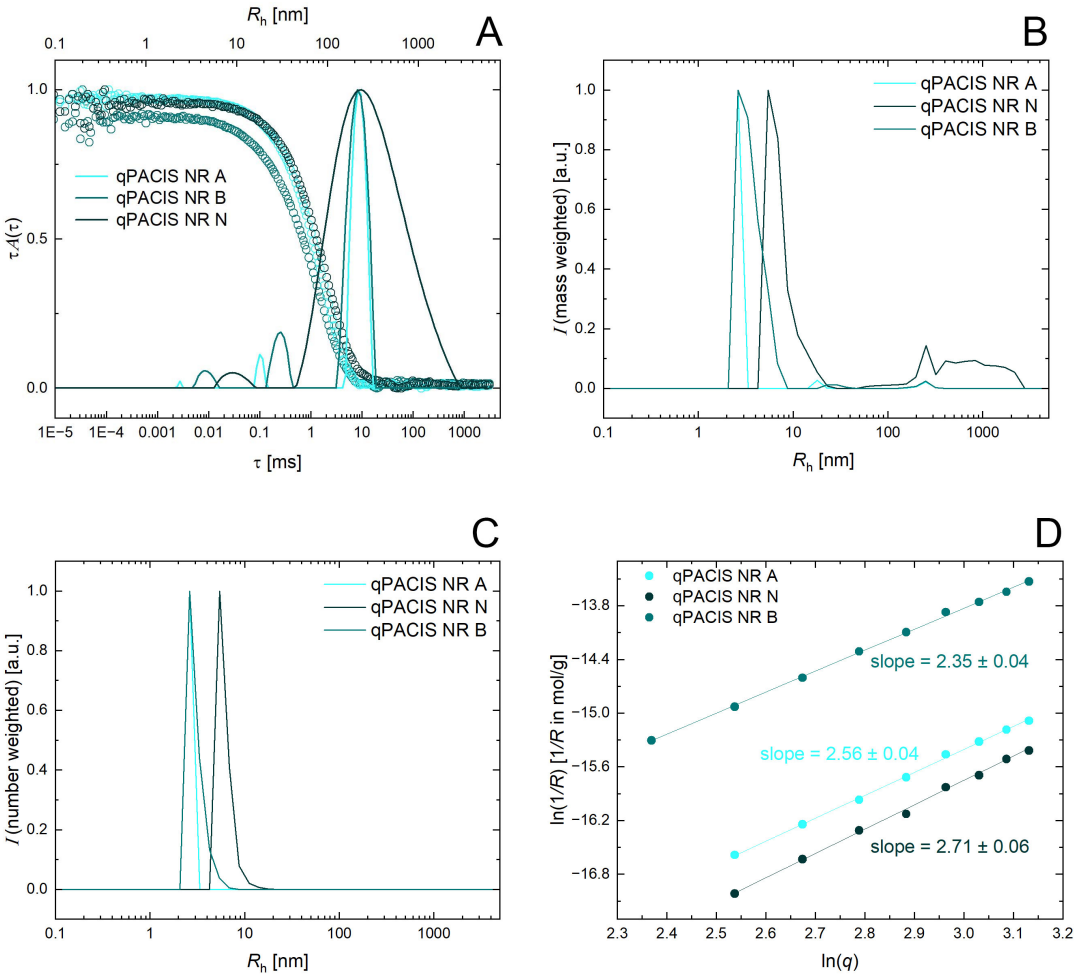

Figure 4.8 DLS correlation functions and intensity weighted (A), mass weighted (B), number weighted distribution functions of hydrodynamic radius R_h (C), plot $\ln I(q)$ vs. $\ln q$ (D) of qPACIS NR in acidic (0.1 M DCl), neutral (0.1 M NaCl in D_2O) and basic (0.1 M NaOD) solution. The error bars are not visible, their size is smaller than the size of the symbols. Square symbols symbolize the values extrapolated to zero angle and zero concentrations.

The intensity weighted distributions of qPACIS NR are displayed in Figure 4.8. The distributions are multimodal. qPACIS NR A and qPACIS NR B have similar position of major peak and differ with position of minor peaks, both of them are trimodal. The distribution of qPACIS NR N is completely different in comparison with two other distributions due to the dispersity of major peak and bimodality. The size of qPACIS NR A major peak is 222 nm. First minor peak contributes little and second peak has size 18 nm. The size of broad major peak of qPACIS NR N is 292 nm and smaller peak has size 9 nm. As mentioned above, this big peak can be caused by dirt or dust. The major peak size of qPACIS NR B is 214 nm. First peak has size 5 nm and second peak has size 30 nm.

The mass weighted distribution that big particles seen in the intensity weighted distributions are probably cause by some impurities, because those peaks are not negligible. The qPACIS NR A distribution is composed from three peaks. The size of major peak is 3 nm. Second peak has size 18 nm and third peak has size 242 nm. The distribution of qPACIS NR N contains two peaks, one with size

7 nm and second with size 569 nm. The second peak is broaden, which means the distribution of different sizes is wider. qPACIS NR B has three peaks with size 3 nm, 26.83 nm and 238 nm.

The number weighted distribution is much simpler. All distributions are monomodal. The size of qPACIS NR A is 3 nm. qPACIS NR N has size 6 nm and qPACIS NR B has size 3 nm.

The plot $\ln I(q)$ vs. $\ln q$ shows that all slope values of qPACIS NR are bigger than 2, which means the dependencies has power law and do not belong to the Guinier area. The fit is not relevant for this particles, because the particle sizes are so big. Moreover, the values of R_g can not be evaluated. As the value of slopes is 2, all scattering particles are compact and on LS scale is visible inner structure of aggregates.

The R_g and R_h is not consistently increasing or decreasing with the change of pH and there is no the same trend for all pH environments and all molecular weights.

The R_g is increasing with the higher pH for PISC 7k, PISC 75k and for PACIS 75k. PISC NR, PACIS NR and qPACIS NR have the biggest aggregates in neutral solution. However, this can be caused by bigger dispersity of starting PIS NR. PACIS 7k shows that in neutral solutions, the aggregates have the smallest size. However, a lot of PE do not belong to the Guinier area. Hence, the comparisons may be prone to the error.

The R_h of PISC 75k, PACIS NR, qPACIS NR is increasing with the higher pH. PISC 7k and PACIS 75k have the smallest size in the neutral pH. PISC NR and PACIS 7k have the biggest size in the neutral pH.

The short PEs do not have the opportunity to conformationally stabilize, because they are relatively stiff. Hence, they are strained in case of conformation and they tend not to form neat, small aggregates with other chains. The longer PE chains can form coils and the surface of the formed coil can interact with other coils. Those PE chains are more flexible and more stabilized, because they can conformationaly stabilize. Therefore, the PEs of higher molecular weight form smaller aggregates, than those of lower molecular weights.

Usually, PE show in same pH conditions similar behaviour. Used PE contain both positively and negatively charged groups, so we can refer them as PZ. When PZ contain basic group (as our PE amines), in acidic pH they are protonated. As a result, PZ have excess positive charge on their chain. In case of conformation, it causes more extended structure due to the higher repulsion between positively charged groups. In neutral pH, amines and carboxylic groups are both charged. So, PE should have minimal charge and it can promote hydrogen bonding in this state. Hence, the polymer conformation may be more compact, because of possibility of intramolecular attractions. In basic pH, acidic groups have negative charge, which leads to an excess negative charge, because amines are deprotonated. In case of conformation, the polymers may show expanded conformation. The negatively charged groups electrostaticly repel from each other. Our PE do not showcase similar behaviour. Unfortunately, there is seen no trend. The explanation for that may be in more complex electrostatic behaviour and also some role plays presence of unmodified starting polymer PIS.

4.3 Associates size determination by static light and small angle X-ray scattering

SAXS measurements were carried out to observe overall structure of our samples, which create aggregates. The structure of solution can be determined at the nm scale. Figures of all fitted PE are displayed in Figure 4.9.

For PACIS NR A, N and B, we can see slight increase for $q < 0.4$ nm^{-1}. The fitting of SAXS was restricted by SLS data in the q range starting from 0.01 to 0.03 nm^{-1}. The SAXS and SLS data were fitted simultaneously by a model using Gaussian coil as a form factor and mass fractal with an exponential cut-off as a structure factor. Gaussian coil is given by equations 4.1 and 4.2.

$$I_{\text{Gauss}}(q) = I_0 2\frac{exp(-u) + u - 1}{u^2} \tag{4.1}$$

$$u = q^2 R_g^2 \tag{4.2}$$

Structure factor is given by equation 4.3

$$S_{\text{Exp}}(q,\xi,D,r_0) = 1 + \frac{D\Gamma(D-1)\sin([D-1]\arctan(q\xi))}{(qr_0)^D[1+\frac{1}{q^2\xi^2}]^{\frac{D-1}{2}}} \tag{4.3}$$

where ξ is cut-off length for the fractal correlations, D is the fractal dimension, r_0 is the characteristic dimension of individual scattering objects and Γ is the gamma function.

The scattering function, which is used for fitting the data, is a product of equations 4.1 and 4.3. Input parameter for this model is also the fractal dimension D, which was fixed parameter as $D = 2.5$. It is a limit for dilute solutions and represents reaction limited cluster aggregation (RLCA), where is present repulsion between particles.[58] The RLCA is not simply controlled by diffusion, where the particles irreversibly stick on each other within the first collision, but it takes multiple steps in order to stick. As a result, the fractal dimension D is greater, because it makes the structure more compact. PACIS NR N is such a large aggregate, that it does not fit into the LS range of q-s and it shows the power dependence. PACIS NR A and PACIS NR B behave analogously, excluding PACIS NR A is bigger than PACIS NR B.

For PISC NR N and B, we can see increase for $q < 0.3$ nm^{-1}. For PISC NR A, the increase is steeper for $q < 0.5$ nm^{-1}. PISC NR N and PISC NR B data were fitted with the same model as PACIS NR data. However, PISC NR A was fitted with the different model, where the aggregates were growing from compact spheres and free coils coexist (do not interact) with the formed aggregates. They were added into the model as a separate component. This model is not reliable, because the Guinier regime is not fully developed. From this curve is visible, that the aggregates are more dense or even precipitated, which means, it is not possible to differentiate individual particles, which form the associates.

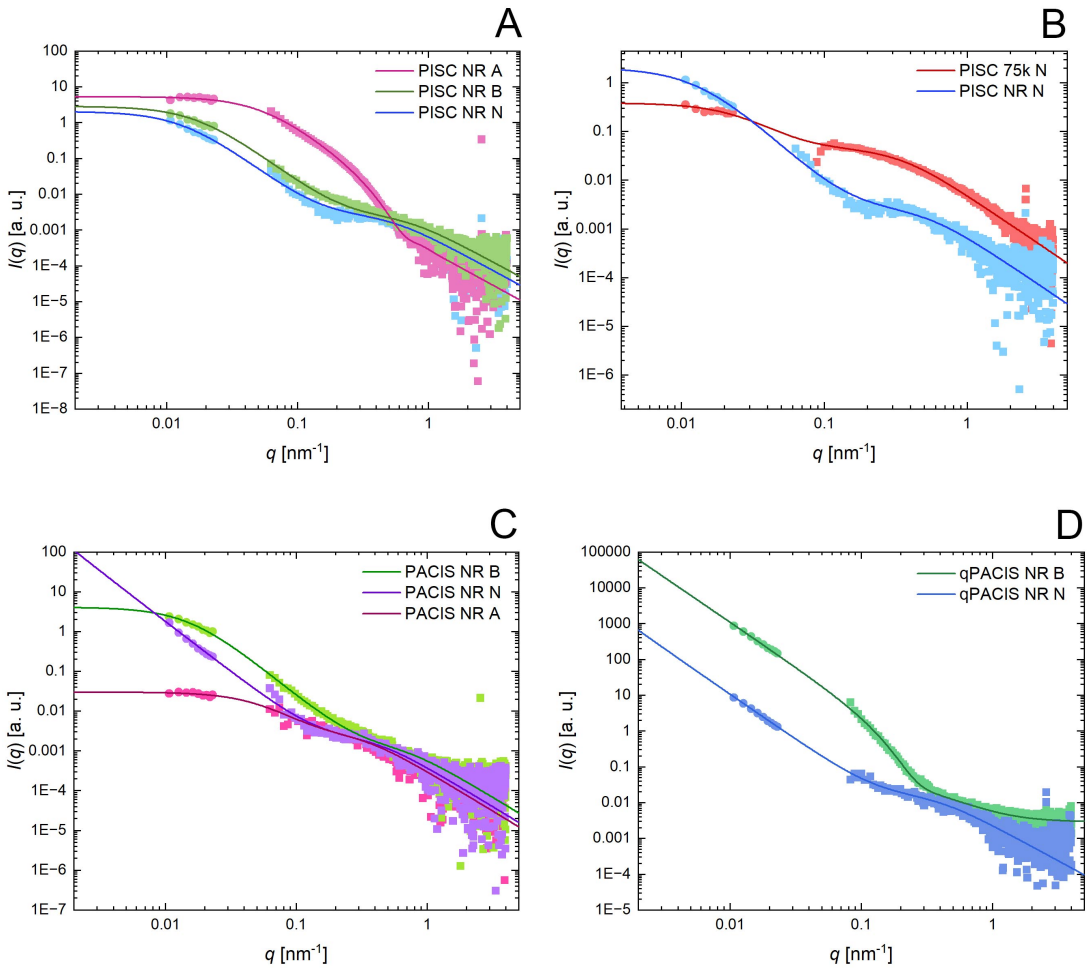

Figure 4.9 SLS (circles) and SAXS (squares) data for PISC NR (A) and PACIS NR (C) in 0.1 M DCl (A), in 0.1 M NaCl (N) and in 0.1 M NaOD (B), PISC NR and 75k (B) and qPACIS (D) in 0.1 M NaCl (N) and in 0.1 M NaOD (B).

Figure 4.9 B displays the comprasion of PISC NR N and PISC 75k N. For both were used the same model as for PACIS NR. PISC 75k N increases gradually from large q-s.

qPACIS NR N and qPACIS NR B are displayed in Figure 4.9 D. qPACIS NR N shows the increase from $q < 0.3$ nm^{-1}, the model for fitting was used the same as on PACIS NR-s. qPACIS NR B increases more steeply from the same values - $q < 0.3$ nm^{-1}, on which was used different model. This model was more complicated, as before the structure factor is described by mass fractal with exponential cut-off and has two other contributions.

$$I(q) = A \exp(-\frac{R_g^2 q^2}{3}) \tag{4.4}$$

First contribution (4.4) utilizes uniform Gaussian coils with extended Guinier law. A is a pre-factor, which is characteristic for the apparent particle shape (or in other words, the dimensionality). The pre-factor describes the excess differential cross-section per unit mass and it's unit is [cm^{2}g^{-1}]. This contributions is used for small q-s, because the curve does not limit to the constant value in Rayleigh

regime, but it limits to the power dependence. Second contribution utilizes uniform Gaussian coils. It's equation is given by 4.1.

The differences between pH conditions can very much affect the contrast and also the counterion condensation is probably the reason of different behaviour. Moreover, highly important factor, which influence aggregation, is that 20 % of monomeric units are not modified. Hence, this part of polymer is hydrophobic. However, this should be visible in longer length scales.

The values of fitted parameters can be find in Table 4.2.

Table 4.2 Forward scattering intensity for one coil $I(0)$, radius of gyration R_g, cut-off length for the fractal correlations ξ and characteristic dimension of individual scattering objects r_0.

Polymer	$I(0)$ [a.u.]	R_g [nm]	ξ [nm]	r_0 [nm]
PISC NR A	13.3	10	18	0.1
PISC NR N	2.76	3	71	8
PISC NR B	2.67	2	55	5
PISC 75k N	46.07	4	33	24
PACIS NR A	2.85	4	17	11
PACIS NR N	2.33	3	∞	8
PACIS NR B	1.45	2	61	4
qPACIS NR N	17.17	4	∞	9
qPACIS NR B	9.75	3	∞	2

The radius of gyration R_g value of PISC NR A is large, in comparison with its r_0, which have to be bigger than R_g. Moreover, r_0 is physically irrelevantly small. Determination of the inner structure of the associates using this model is not reliable. The associates seem to be dense, because it was not possible to identify single constituent of the associate. From Figure 4.9 A can be concluded that PISC NR A was not in the same state in case of measuring SAXS and SLS, because SLS shows smaller particles than SAXS, which means the solution started precipitating within long SAXS measurement. The precipitation of the sample was observed after one day, which could significantly affected SAXS measurements. Also, the cut-off lengths for the fractal correlations ξ for PACIS NR N, qPACIS NR N and qPACIS NR B are not physically relevant. Hence, it can be seen from fits for these three PEs that the fit does not limit to constant, but it follows power law.

4.4 Associates zeta potential determination

We measured ZP of our samples in aqueous solutions, with starting concentration of PEs 1 mg/ml, by changing the pH of the solutions 1 to 12. The measured values are displayed, as a dependence on pH in Figure 4.10. The ionization state of PEs is changing by alternation of pH. The determined pKa values can be found in section 4.1. However, those values are established for a low molecular compound resembling monomer unit of PACIS. Hence, real pKa values can be shifted in regards to the studied polymers. The overall net charge of the PISC molecules is

negative, because of the presence of sulfamate group, which is ionized throughout the whole pH range. Those sulfamate groups are present on the surface of the studied associates, which gives raise to their highly negative ZP values for all three studied molecular weights at all pH range. After the acid cleavage of the sulfamate group, the ZP for PACIS varies from positive values in the acidic pH to negative values in the basic pH. Below the pH = 3.63 (pKa of the carboxyl) both the amine and carboxyl groups are protonated, which leads to the overall positive net charge of the formed associates. Above this pH carboxyl groups get deprotonated, leading to overall neutral charge of the polymer with both amine and carboxyl groups being ionized. Since the charges carried by those pendant groups at adjacent carbons are opposite, it leads to electrostatic attraction effects and promotes aggregation. Above the pH = 10.12 (pK_a of the amine) both carboxyl and amine groups are deprotonated and the overall net charge of the polymers is negative. qPACIS contains a quaternized amino group which carries a permanent positive charge throughout the whole pH range. As before, the carboxylic group is deprotonized in basic environment and then qPACIS gains net neutral charge. However, because of the incomplete modification of the chemical structure above pH = 4.52 ZP drops below zero. Moreover, the hydroxyl ions can be adsorbed on the surface of the associates, giving raise to the negative ZP as oppose to hydrogen ions which lead to in raise of positive ZP.

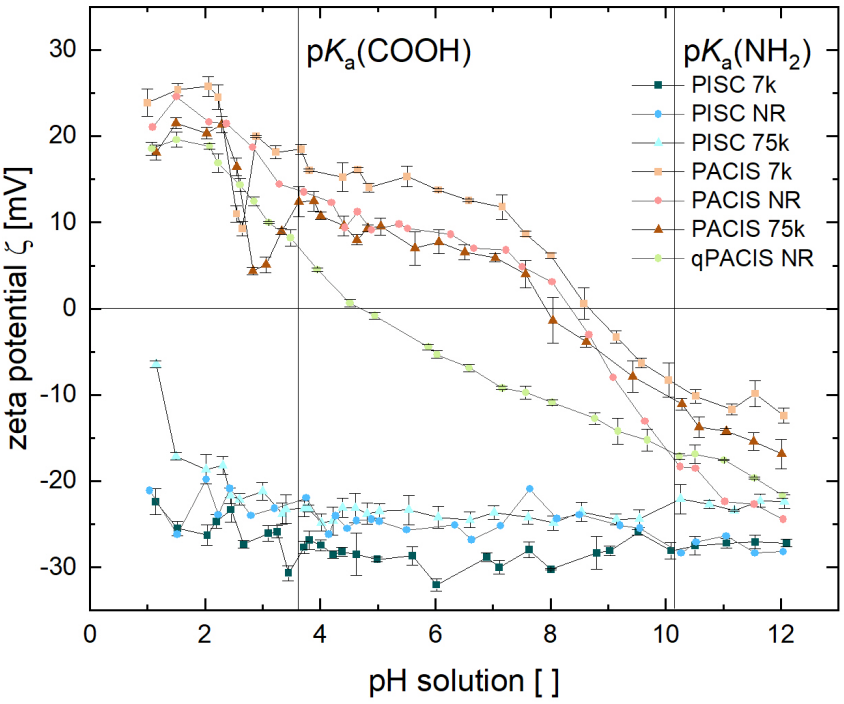

Figure 4.10 Dependence of ZP on pH of the solution of measured PE. The line connecting measured points is used for better visualization.

All used PE contain hydrophobic parts, because the post polymerization process was not completely carried out for all monomeric units. The unmodified

hydrophobic PIS domains play role in aggregation and can have an effect on ZP. One point of view is that hydrophobic parts are in the middle of assembled particle and all charged groups are exposed. However, based on LS measurements, the particles group into bigger assemblies. The interactions between the particles include hydrogen bonding of carboxylic groups with water molecules. Even hydrogen bonds can be created through several molecules of water and this solvation layer can be conjunctive for several carboxylic groups. Moreover, the studied associates are relatively large and it can be caused by the insertion of molecules of solvent or the free ions present in the solution into the outer structure of the associate. The inserted free ions can significantly influence the size of the aggregates through the electrostatic interactions.

Conclusion

In this bachelors thesis three different PEs were studied - PISC, PACIS and qPACIS. PISC and PACIS were investigated in three different molecular weights - 7.5, 38 and 75.5 kDa. Additionally, qPACIS was studied in one molecular weight - 38 kDa. All PE were prepared in three different pH environments - at acidic, neutral and basic pH to observe changes in PE behaviour and size properties.

The LS scattering measurements were carried out for all PEs - specifically, DLS and SLS measurements in order to obtain the diffusion coefficients, and consequently the particle sizes.

The SAXS measurements were performed for chosen PEs in order to obtain information about particle sizes and the measured data from SAXS were connected with SLS data.

The zeta potential measurements were carried out in order to observe how the studied PEs behave in different pH environments in more detail and to investigate the particle charge on the surface of the aggregate.

DLS measurements show that our particles form bigger associates or multichain domains, but number of them was not high as was seen from number weighted distributions functions of R_h. The smaller values of sizes belong to single chains or couple of chains interacting with each other. Most of the hydrodynamic radius distributions are multimodal.

As the PEs have general tendency to showcase complex behaviour, the DLS distributions were multimodal in many cases, which made them complicated to interpret. The complex behaviour is caused by the contributions of different particles (polyions, counterions, co-ions and solvent) or by dynamic modes present in the system. Specifically, slow mode, which corresponds to the polyion diffusion and fast mode, which corresponds to the ions diffusion.[59] The analysis of slow and fast mode can be carried out in the future in order to understand the behavior of studied PE in more detail.

For some of the samples, the particle size exceeded the threshold suitable for LS analysis and those did not belong to the Guinier area. To ensure the correct evaluation of those data smaller values of q^2 would be needed, which can be obtained from wide angle X-ray scattering.

The chains of studied PEs interact with other chains via hydrogen bonding and also electrostatic repulsion, which play an important role in the aggregation process. In polymer chains are also present hydrophobic parts, which are unmodified monomer units of starting polymer PIS and they can form hydrophobic domains.

Our hypothesis was that PE with bigger molecular weight form bigger aggregates. Interestingly, this was not confirmed, but the opposite with comparison of sizes in basic solution. The short PEs do not have the opportunity to conformationally stabilize, because they are relatively stiff. Hence, they are strained in case of conformation and they tend not to form neat, small associates with other chains. The longer PE chains can form coils and the surface of the formed coil can interact with other coils. Those PE chains are more flexible and more stabilized due to conformational stabilization. Therefore, the PEs of higher molecular weight form smaller associates, than those of lower molecular weights.

Used PE do not show typical PZ behaviour in case of pH-dependence and

conformation. This could be caused by more complex behaviour in terms of electrostatic interactions and non-negligible factor is presence of unmodified monomer units of starting polymer PIS, which can influence conformation.

References

1. Schanze, Kirk S; Shelton, Abigail H. Functional Polyelectrolytes. *Langmuir*. 2009, vol. 25, no. 24, pp. 13698–13702. issn 0743-7463.
2. Yeh, Li-Hsien; Hsu, Jyh-Ping; Qian, Shizhi; Tseng, Shiojenn. Counterion condensation in pH-regulated polyelectrolytes. *Electrochemistry communications*. 2012, vol. 19, no. 1, pp. 97–100. issn 1388-2481.
3. Zohuriaan-Mehr, M. J.; Omidian, H.; Doroudiani, S.; Kabiri, K. Advances in non-hygienic applications of superabsorbent hydrogel materials. *Journal of materials science*. 2010, vol. 45, no. 21, pp. 5711–5735. issn 0022-2461.
4. Sharma, Varsha; Sundaramurthy, Anandhakumar. Multilayer capsules made of weak polyelectrolytes: A review on the preparation, functionalization and applications in drug delivery. *Beilstein journal of nanotechnology*. 2020, vol. 11, no. 1, pp. 508–532. issn 2190-4286.
5. Singh, Jagtar; Nayak, Pallavi. pH-responsive polymers for drug delivery: Trends and opportunities. *Journal of polymer science (2020)*. 2023, vol. 61, no. 22, pp. 2828–2850. issn 2642-4150.
6. Uchman, Mariusz; Procházka, Karel; Štěpánek, Miroslav; Mountrichas, Grigoris; Pispas, Stergios; Špírková, Milena; Walther, Andreas. pH-Dependent Self-Assembly of Polystyrene-block-Poly((sulfamate-carboxylate)isoprene) Copolymer in Aqueous Media. *Langmuir*. 2008, vol. 24, no. 20, pp. 12017–12025. issn 0743-7463.
7. Dobrynin, Andrey V. Polyelectrolytes: On the doorsteps of the second century. *Polymer (Guilford)*. 2020, vol. 202, pp. 122714–. issn 0032-3861.
8. Filippov, Sergey K; Khusnutdinov, Ramil; Murmiliuk, Anastasiia; Inam, Wali; Zakharova, Lucia Ya; Zhang, Hongbo; Khutoryanskiy, Vitaliy V. Dynamic light scattering and transmission electron microscopy in drug delivery: a roadmap for correct characterization of nanoparticles and interpretation of results. *Materials horizons*. 2023, vol. 1, no. 12, pp. 5354–537. issn 2051-6347.
9. Uchman, Mariusz; Procházka, Karel; Gatsouli, Katerina; Pispas, Stergios; Špírková, Milena. CdS-containing nano-assemblies of double hydrophilic block copolymers in water. *Colloid and polymer science*. 2011, vol. 289, no. 9, pp. 1045–1053. issn 0303-402X.
10. Uchman, Mariusz; Štěpánek, Miroslav; Procházka, Karel; Mountrichas, Grigoris; Pispas, Stergios; Voets, Ilja K; Walther, Andreas. Multicompartment Nanoparticles Formed by a Heparin-Mimicking Block Terpolymer in Aqueous Solutions. *Macromolecules*. 2009, vol. 42, no. 15, pp. 5605–5613. issn 0024-9297.
11. Dobrynin, Andrey V.; Rubinstein, Michael. Theory of polyelectrolytes in solutions and at surfaces. *Progress in polymer science*. 2005, vol. 30, no. 11, pp. 1049–1118. issn 0079-6700.

12. Bjerrum, N. Ionic association. I. Influence of ionic association on the activity of ions. *Mat. Fys. Medd. K. Dan. Vidensk. Selsk.* 1926, vol. 7, pp. 1–48.

13. Matsuda, Yasuhiro; Kobayashi, Motoyasu; Annaka, Masahiko; Ishihara, Kazuhiko; Takahara, Atsushi. Dimensions of a Free Linear Polymer and Polymer Immobilized on Silica Nanoparticles of a Zwitterionic Polymer in Aqueous Solutions with Various Ionic Strengths. *Langmuir*. 2008, vol. 24, no. 16, pp. 8772–8778. ISSN 0743-7463.

14. Delgado, Jose D; Schlenoff, Joseph B. Static and Dynamic Solution Behavior of a Polyzwitterion Using a Hofmeister Salt Series. *Macromolecules*. 2017, vol. 50, no. 11, pp. 4454–4464. ISSN 0024-9297.

15. Elliott, Gerald F; Hodson, Stuart A. Cornea, and the swelling of polyelectrolyte gels of biological interest. *Reports on progress in physics*. 1998, vol. 61, no. 10, pp. 1325–1365. ISSN 0034-4885.

16. Zhong, Peihua; Wang, Jun; Wang, Xiaoxian; Liu, Jiaping; Li, Zhen; Zhou, Yichuan. Comparison of different approaches for testing sorption by a superabsorbent polymer to be used in cement-based materials. *Materials*. 2020, vol. 13, no. 21, pp. 1–17. ISSN 1996-1944.

17. Fuoss, Raymond M. Viscosity function for polyelectrolytes. *Journal of Polymer Science*. 1948, vol. 3, no. 4, pp. 603–604. ISSN 0022-3832.

18. Doi, Masao; Birman, J.; Edwards, S. F. *The theory of polymer dynamics*. The theory of polymer dynamics. Oxford: Oxford Univ. Press, 1998. The international series of monographs on physics ; Sv.73. ISBN 0-19-852033-6.

19. Gennes, Pierre-Gilles de. *Scaling concepts in polymer physics*. Scaling concepts in polymer physics. Ithaca: Cornell University Press, 1979. ISBN 978-0-8014-1203-5.

20. Rubinstein, Michael; Colby, Ralph H. *Polymer physics*. Polymer physics. Oxford: Oxford University Press, 2003. ISBN 0-19-852059-X.

21. Bohidar, Himadri B. *Fundamentals of polymer physics and molecular biophysics*. Fundamentals of polymer physics and molecular biophysics. Cambridge: Cambridge University Press, 2015. ISBN 1-316-09311-5.

22. Katchalsky, Aharon; Spitnik, Pnina. Potentiometric titrations of polymethacrylic acid. *Journal of Polymer Science*. 1947, vol. 2, no. 4, pp. 432–446.

23. Tanford, Charles. *Physical chemistry of macromolecules*. Physical chemistry of macromolecules. New York: Wiley, 1961.

24. Geoghegan, Mark. Weak polyelectrolyte brushes. *Soft matter*. 2022, vol. 18, no. 13, pp. 2500–2511. ISSN 1744-683X.

25. Nelson, David L. (David Lee); Cox, Michael M.; Hoskins, Aaron A.; Lehninger, Albert L. *Lehninger principles of biochemistry*. Lehninger principles of biochemistry. Eight edition. New York: Macmillan international, 2021. ISBN 978-1-319-38149-3.

26. Guzmán, Eduardo; Ortega, Francisco; Baghdadli, Nawel; Cazeneuve, Colette; Luengo, Gustavo S; Rubio, Ramón G. Adsorption of Conditioning Polymers on Solid Substrates with Different Charge Density. *ACS applied materials & interfaces*. 2011, vol. 3, no. 8, pp. 3181–3188. issn 1944-8244.

27. Dautzenberg, Herbert; Jaeger, Werner. Effect of charge density on the formation and salt stability of polyelectrolyte complexes. *Macromolecular chemistry and physics*. 2002, vol. 203, no. 14, pp. 2095–2102. issn 1022-1352.

28. Haag, Stephanie L.; Bernards, Matthew T. Polyampholyte hydrogels in biomedical applications. *Gels*. 2017, vol. 3, no. 4, pp. 41–. issn 2310-2861.

29. Laschewsky, André. Structures and synthesis of zwitterionic polymers. *Polymers*. 2014, vol. 6, no. 5, pp. 1544–1601. issn 2073-4360.

30. Li, Qingsi; Wen, Chiyu; Yang, Jing; Zhou, Xianchi; Zhu, Yingnan; Zheng, Jie; Cheng, Gang; Bai, Jie; Xu, Tong; Ji, Jian; Jiang, Shaoyi; Zhang, Lei; Zhang, Peng. Zwitterionic Biomaterials. *Chemical reviews*. 2022, vol. 122, no. 23, pp. 17073–17154. issn 0009-2665.

31. Laughlin, Robert G. Fundamentals of the zwitterionic hydrophilic group. *Langmuir*. 1991, vol. 7, no. 5, pp. 842–847. issn 0743-7463.

32. Kudaibergenov, Sarkyt; Jaeger, Werner; Laschewsky, Andre. Polymeric betaines: synthesis, characterization, and application. *Supramolecular polymers polymeric betains oligomers*. 2006, pp. 157–224.

33. Nakaya, Tadao; Li, Yu-Jun. Phospholipid polymers. *Progress in Polymer Science*. 1999, vol. 24, no. 1, pp. 143–181.

34. Hoffman, Allan S.; Stayton, Patrick S.; Bulmus, Volga; Chen, Guohua; Chen, Jingping; Cheung, Chuck; Chilkoti, Ashutosh; Ding, Zhongli; Dong, Liangchang; Fong, Robin; Lackey, Chantal A.; Long, Cynthia J.; Miura, Morikazu; Morris, John E.; Murthy, Niren; Nabeshima, Yoshikuni; Park, Tae Gwan; Press, Ollie W.; Shimoboji, Tsuyoshi; Shoemaker, Sara; Yang, Heung Joon; Monji, Nobuo; Nowinski, Robert C.; Cole, Carole Ann; Priest, John H.; Harris, J. Milton; Nakamae, Katsuhiko; Nishino, Takashi; Miyata, Takashi. Really smart bioconjugates of smart polymers and receptor proteins. *Journal of biomedical materials research*. 2000, vol. 52, no. 4, pp. 577–586. issn 0021-9304.

35. Bermudez, Harry; Brannan, Aaron K; Hammer, Daniel A; Bates, Frank S; Discher, Dennis E. Molecular Weight Dependence of Polymersome Membrane Structure, Elasticity, and Stability. *Macromolecules*. 2002, vol. 35, no. 21, pp. 8203–8208. issn 0024-9297.

36. Lowe, Andrew B; McCormick, Charles L. Synthesis and Solution Properties of Zwitterionic Polymers. *Chemical reviews*. 2002, vol. 102, no. 11, pp. 4177–4190. issn 0009-2665.

37. Laschewsky, André. Recent trends in the synthesis of polyelectrolytes. *Current opinion in colloid & interface science*. 2012, vol. 17, no. 2, pp. 56–63. issn 1359-0294.

38. Comparison and Classification of Controlled/Living Radical Polymerizations. In: *American Chemical Society eBooks*. American Chemical Society, [n.d.].

39. ØGENDAL, Lars Holm. *Light Scattering Demystified: Theory and Practice*. University of Copenhagen. 2017.

40. SCHÄRTL, Wolfgang. *Light scattering from polymer solutions and nanoparticle dispersions*. Light scattering from polymer solutions and nanoparticle dispersions. Berlin ; Springer, 2007. Springer laboratory manuals in polymer science. ISBN 9783540719502.

41. KOLTZENBURG, Sebastian; MASKOS, Michael; NUYKEN, Oskar. *Polymer chemistry*. Polymer chemistry. Berlin: Springer Verlag, 2017. ISBN 978-3-662-49277-2.

42. HAWE, Andrea; HULSE, Wendy L.; JISKOOT, Wim; FORBES, Robert T. Taylor Dispersion Analysis Compared to Dynamic Light Scattering for the Size Analysis of Therapeutic Peptides and Proteins and Their Aggregates. *Pharmaceutical research*. 2011, vol. 28, no. 9, pp. 2302–2310. ISSN 0724-8741.

43. STETEFELD, Jörg; MCKENNA, Sean A.; PATEL, Trushar R. Dynamic light scattering: a practical guide and applications in biomedical sciences. *Biophysical reviews*. 2016, vol. 8, no. 4, pp. 409–427. ISSN 1867-2450.

44. BHATTACHARJEE, Sourav. DLS and zeta potential – What they are and what they are not? *Journal of controlled release*. 2016, vol. 235, pp. 337–351. ISSN 0168-3659.

45. UCHMAN, Mariusz; ŠTĚPÁNEK, Miroslav; PRÉVOST, Sylvain; ANGELOV, Borislav; BEDNÁR, Jan; APPAVOU, Marie-Sousai; GRADZIELSKI, Michael; PROCHÁZKA, Karel. Coassembly of Poly(ethylene oxide)-block-poly(methacrylic acid) and N-Dodecylpyridinium Chloride in Aqueous Solutions Leading to Ordered Micellar Assemblies within Copolymer Aggregates. *Macromolecules*. 2012, vol. 45, no. 16, pp. 6471–6480. ISSN 0024-9297.

46. PECORA, R. Dynamic Light Scattering Measurement of Nanometer Particles in Liquids. *Journal of nanoparticle research : an interdisciplinary forum for nanoscale science and technology*. 2000, vol. 2, no. 2, pp. 123–. ISSN 1388-0764.

47. SEECK, Oliver H. *X-ray diffraction : modern experimental techniques*. X-ray diffraction : modern experimental techniques. Boca Raton, Florida: Pan Stanford Publishing, 2015. ISBN 0-429-07189-2.

48. LIU, Li; BOLDON, Lauren; URQUHART, Melissa; WANG, Xiangyu. Small and Wide Angle X-ray Scattering studies of biological macromolecules in solution. *Journal of visualized experiments*. 2013, no. 71. ISSN 1940-087X.

49. KIKHNEY, Alexey G.; SVERGUN, Dmitri I. A practical guide to small angle X-ray scattering (SAXS) of flexible and intrinsically disordered proteins. *FEBS letters*. 2015, vol. 589, no. 19, pp. 2570–2577. ISSN 0014-5793.

50. GRÄWERT, Melissa; SVERGUN, Dmitri. A beginner's guide to solution small-angle X-ray scattering (SAXS). *The Biochemist*. 2020, vol. 42, pp. 36–42. Available from DOI: 10.1042/BIO04201036.

51. Putnam, Christopher D.; Hammel, Michal; Hura, Greg L.; Tainer, John A. X-ray solution scattering (SAXS) combined with crystallography and computation: defining accurate macromolecular structures, conformations and assemblies in solution. *Quarterly reviews of biophysics*. 2007, vol. 40, no. 3, pp. 191–285. issn 0033-5835.

52. Lindner, Peter; Zemb, Thomas. *Neutrons, X-rays, and light : scattering methods applied to soft condensed matter*. Neutrons, X-rays, and light : scattering methods applied to soft condensed matter. Amsterdam: Elsevier, 2002. isbn 0-444-51122-9.

53. Kumar, Ajeet; Dixit, Chandra Kumar. 3 - Methods for characterization of nanoparticles. In: *Advances in Nanomedicine for the Delivery of Therapeutic Nucleic Acids*. Elsevier Ltd, 2017, pp. 43–58. isbn 0081005571.

54. Cossio, Gabriel; Yu, Edward T. Zeta Potential Dependent Self-Assembly for Very Large Area Nanosphere Lithography. *Nano letters*. 2020, vol. 20, no. 7, pp. 5090–5096. issn 1530-6984.

55. Malvern, Worldwide Instruments. *Zeta potential - An introduction in 30 minutes*. 2015. Available also from: `https://www.research.colostate.edu/wp-content/uploads/2018/11/ZetaPotential-Introduction-in-30min-Malvern.pdf`. [Online; accessed 8-April-2024].

56. Nová, Lucie; Uhlík, Filip; Košovan, Peter. Local pH and effective pK A of weak polyelectrolytes - insights from computer simulations. *Physical chemistry chemical physics : PCCP*. 2017, vol. 19, no. 22, pp. 14376–14387. issn 1463-9076.

57. Hsu, Hsuan-Pei; Lee, Eric. Counterion condensation of a polyelectrolyte. *Electrochemistry communications*. 2012, vol. 15, no. 1, pp. 59–62. issn 1388-2481.

58. Jungblut, Swetlana; Joswig, Jan Ole; Eychmüller, Alexander. Diffusion- and reaction-limited cluster aggregation revisited. *Physical chemistry chemical physics : PCCP*. 2019, vol. 21, no. 10, pp. 5723–5729. issn 1463-9076.

59. Sedlak, Marian. What Can Be Seen by Static and Dynamic Light Scattering in Polyelectrolyte Solutions and Mixtures? *Langmuir*. 1999, vol. 15, no. 12, pp. 4045–4051. issn 0743-7463.

List of Figures

1.1 Polyelectrolyte chain. 3
1.2 Concentration regimes. 5
1.3 Strong and weak polyelectrolytes. 6
1.4 Different types of polyelectrolytes. 7
1.5 Polyelectrolyte type division. 7
1.6 Potential distribution of ionic groups in polyzwitterions. 8
1.7 Interference pattern of the light 10
1.8 DLS vs. SLS. 11
1.9 Scattering vector. 12
1.10 Details observed on q-scale. 12
1.11 The buffer data subtraction from the sample data. 15
1.12 Diagram of processes in colloidal dispersion. 17
1.13 Schematic representation of zeta potential. 18

3.1 Synthetic pathway of studied polyelectrolytes 20

4.1 Ionization schemes of used PEs. 23
4.2 DLS and SLS of PISC 7k. 26
4.3 DLS and SLS of PISC NR. 27
4.4 DLS and SLS of PISC 75k. 29
4.5 DLS and SLS of PACIS 7k. 30
4.6 DLS and SLS of PACIS NR. 32
4.7 DLS and SLS of PACIS 75k. 33
4.8 DLS and SLS of qPACIS NR. 34
4.9 SAXS of PISC NR, PACIS NR, PISC NR and 75k and qPACIS NR N and B. 37
4.10 Zeta ζ potential results 39

List of Tables

4.1 Radius of gyration R_g obtained from Guinier plots from the measurements at 90° 24
4.2 SAXS fitted parameters. 38